Nanomaterials and Films for Polymer Electrolyte Membrane Fuel Cells and Solid Oxide Cells by Flame Spray Pyrolysis

Suriya Venkatesan[1], Jens Mitzel[1, *], Karsten Wegner[2, 3], Remi Costa[1], Pawel Gazdzicki[1], Kaspar Andreas Friedrich[1, 4, *]

[1] Department of Electrochemical Energy Technology, Institute of Engineering Thermodynamics, German Aerospace Centre (DLR), D-70569 Stuttgart, Germany

[2] Particle Technology Laboratory, Department of Mechanical and Process Engineering, ETH Zurich, CH-8092 Zurich, Switzerland

[3] ParteQ GmbH, Brunnenstrasse, D-76316 Malsch, Germany

[4] Institute of Building Energetics, Thermal Engineering and Energy Storage (IGTE), University of Stuttgart, D-70569 Stuttgart, Germany

* = Corresponding author(s): Jens.Mitzel@dlr.de; Andreas.Friedrich@dlr.de

Abstract:

Significant progress has been achieved in the development of nanomaterials for polymer electrolyte membrane fuel cells (PEMFC) and solid oxide cells (SOC). However, the limited scalability and multi-step processing of the conventional synthesis routes for the electrocatalysts, their supports and thin functional films in general (e.g., co-precipitation and solid-state synthesis) remain a great challenge for inexpensive production of these energy materials and cells. These drawbacks could be overcome by flame spray pyrolysis (FSP), a simple, rapid, scalable and single step fabrication technique. Here, a comprehensive review on flame-based synthesis and deposition techniques with a major focus on FSP for PEMFCs and SOCs is presented. Flame-made materials of practical importance including Pt, Pt alloys, metal-nitrogen-carbon catalysts, perovskites and catalyst support structures, and their performance are discussed along with challenges and opportunities to bridge the gap between materials research and cell development.

Graphical Abstract:

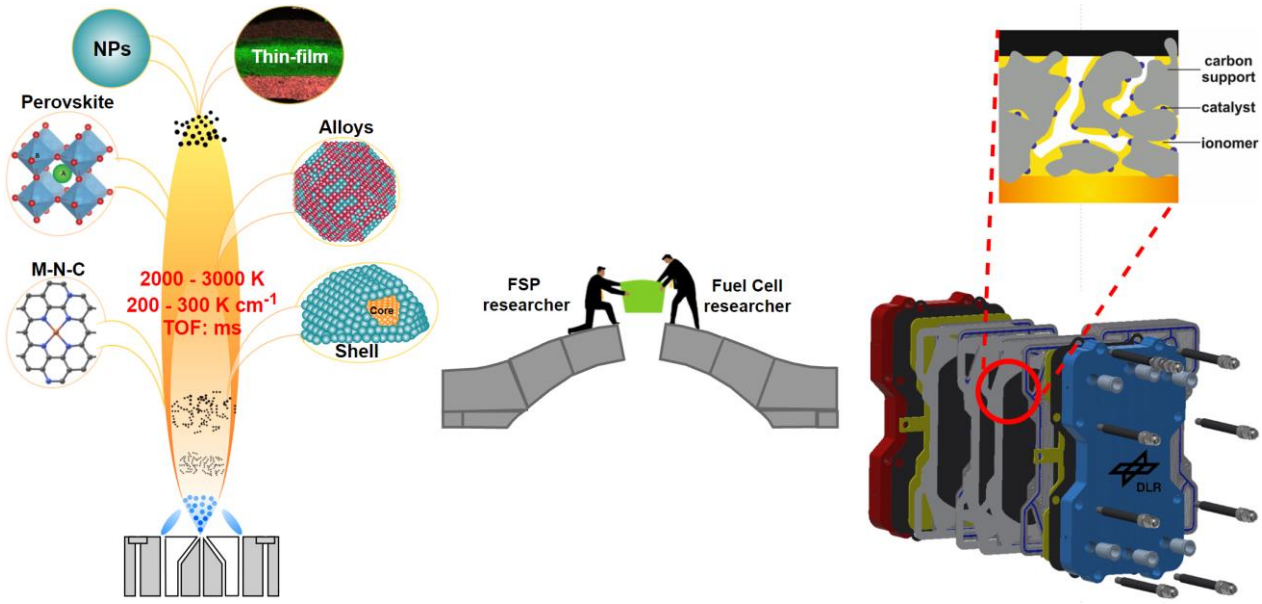

Highlights:

- FSP - a cost-efficient, scalable and single-step synthesis method for nanomaterials
- Progress in FSP-made nanomaterials and thin-films for PEMFC and SOC is reviewed
- Advancement, opportunities and challenges in FSP for cell development are highlighted
- Strategies for the production of next generation materials are recommended

Keywords:

Polymer electrolyte membrane fuel cell, Solid oxide cell, Solid oxide fuel cell, Flame spray pyrolysis, Flame synthesis, Nanomaterial, Thin-film.

Word count: 11437 words (excluding title, authors affiliations, abstract, highlights, keywords, word count, list of abbreviations, figure/table captions, table, declaration of competing interest, acknowledgement, author contributions and list of references).

List of Abbreviations:

AFD	Aerosol flame deposition
BSCF	$Ba_{1-y}Sr_yCo_{1-x}Fe_xO_3$

BZY	$BaZr_{0.8}Y_{0.2}O_{3-\delta}$
CCVD	Combustion chemical vapour deposition
CL	Catalyst layer
CV	Cyclic voltammetry
DMFC	Direct methanol fuel cell
ECSA	Electrochemically active surface area
FAS	Flame aerosol synthesis
FSD	Flame spray deposition
FSP	Flame spray pyrolysis
GDC	$Ce_{0.8}Gd_{0.2}O_{2-\delta}$
GDL	Gas diffusion layer
I/C	ratio of ionomer to carbon
LT-HVOF	Liquid precursor high velocity oxygen fuel flame
LSC	$La_{0.6}Sr_{0.4}CoO_{3-\delta}$
LSCF	$La_{0.6}Sr_{0.4}Co_{0.2}Fe_{0.8}O_{3-\delta}$
LSM	$La_{0.8}Sr_{0.2}MnO_{3+x}$
MEA	Membrane electrode assembly
M-N-C	Metal-Nitrogen-Carbon
ORR	Oxygen reduction reaction
PEMFC	Polymer electrolyte membrane fuel cell
PGM	Platinum group metal
Pt/C	Carbon-supported Pt
PtRu/C	Carbon-supported Pt-Ru alloy
RH	Relative humidity
R_p	Polarization resistance
RSDT	Reactive spray deposition technique
ScCeSZ	$Sc_{0.2}Ce_{0.01}Zr_{0.79}O_2$
ScSZ	$Sc_{0.2}Zr_{0.8}O_2$
SDC	Samarium-doped ceria

SOC	Solid oxide cell
SSA	Specific surface area
SSC	$Sm_{0.5}Sr_{0.5}CoO_3$
TPB	Triple point boundaries
YSZ	$Y_{0.15}Zr_{0.85}O_{2-\delta}$

1. Introduction:

Fuel cells can convert chemical energy from fuels directly to electrical energy using electro-catalytic reactions with system efficiencies of 50 % (low temperature fuel cells) to 60 % (high temperature fuel cells) [1]. Among the various types of fuel cells, PEMFC and SOC are the most promising systems because of low operating temperature and high energy conversion efficiency, respectively [[2], [3]]. In 2019, fuel cell sales totalled for the first time on a gigawatt scale, the majority of them being of PEMFC and SOC types [4].

Thereby, PEMFC technology was mainly deployed in residential, automotive, and portable applications using systems up to a few hundred kilowatts electrical power. Many barriers to widespread commercialization have been overcome during the last decades. Nevertheless, two main challenges remain for the PEMFC technology: durability and costs [5]. In order to master these, challenges new materials with improved stability, lower PGM loading and facilitated manufacturing methods have to be developed [6]. A variety of promising catalyst classes are under investigation for PEMFCs to meet the PGM loading targets [7]. This includes carbon-supported Pt (Pt/C), Pt alloy (PtRu, PtCo, PtNi, etc.), core-shell (Pd@Pt), and non-precious metal catalysts (Fig. 1) [8].

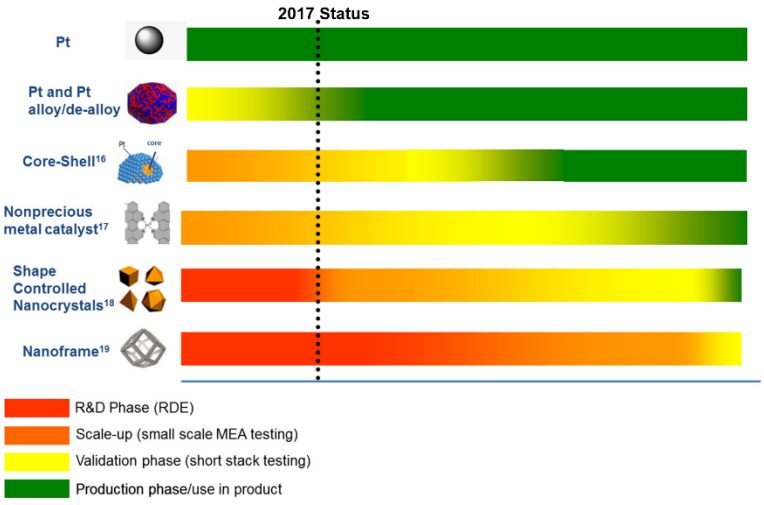

Fig. 1: Development timelines for PEMFC electrocatalysts indicating technology readiness: for Pt, Pt-based alloy, core−shell, nonprecious metal, shape-controlled, and nanoframe ORR electrocatalysts [8]. Adapted from ref. [8] with permission from ACS.

Due to their high efficiency and the fuel flexibility, SOCs are typically applied in stationary, industrial, and power generation modules with a wide power range from a few kilowatts to several megawatts [9]. The key factor for widespread commercialization is the economic competitiveness that must be achieved by lower cost for manufacturing and for materials, such as avoidance of rare-earth elements. A further limiting factor is the high operation temperature of 700-900 °C. Novel and inexpensive electrode and electrolyte materials are required, which maintain their conductive and catalytic properties even at lower temperatures [10].

Consequently, a key hurdle in enabling commercialization of both fuel cell technologies is the cost for synthesizing active nanomaterials for electrodes/electrolyte components and the scalability of fabrication processes without compromising structural and functional features of the nanomaterials [[8], [11], [12]].

Several methods have been investigated for the fabrication of nanostructured fuel cell components, which include conventional chemical synthesis (e.g., co-precipitation, sol-gel, hydrothermal, citrate method, spray pyrolysis), reactive sputtering, plasma spraying followed by spark plasma sintering, powder processing techniques (spin-coating, tape casting, screen printing) and vapour deposition processes [[13], [14], [15]]. However, all of these methods typically require multiple process steps and are often energy-intensive. Furthermore, they are limited by scalability, the high degree of particle agglomeration, and unfavourable microstructures of the deposited thin-films [[13], [14], [15]].

The majority of the above-mentioned synthesis routes for nanomaterials are typically suitable for small-scale batch-type laboratory research [[12], [14]]. For instance, the synthesis of a catalyst by wet chemical methods often takes several hours per batch, excluding the time required for filtration, purification, and drying. The quantity of product usually is in the microgram to gram scale - barely enough to characterize the catalyst *ex-situ* and to perform single cell tests. Scaling up these processes is time-intensive and challenging, as thermal and chemical gradients become more severe and non-linear when the volume of the reaction solution is increased. Moreover, lengthy wet chemical preparation routes can cause the dissolution of nano-catalysts by Ostwald ripening, whereby large particles grow larger and smaller ones shrink. This makes surface area and shape control of the catalysts very challenging and can reduce their activity [[16], [17]]. Furthermore, simultaneous synthesis of supporting structures (e.g. carbons or metal oxides) or functional oxides (e.g. CeO_2 and SnO_2) along with the electrocatalysts and the controlled introduction of dopants (e.g. N, Nb) is not achieved easily with these techniques.

In materials development for SOC components, calcination, sintering, and post-sintering treatments play a crucial role in the performance of the cell and in reducing the operating temperature of SOCs to less than 600 °C [18]. Commonly used materials like yttria-stabilized-zirconia (YSZ), NiO/YSZ cermet electrodes, lanthanum ferrite-based perovskites, doped ceria materials, and their composites are prepared by wet-chemical synthesis that is associated with the previously mentioned drawbacks while two-step solid-state reaction sintering for several hours causes undesirable grain growth, structural instability, and lowers the electrochemically active surface area (ECSA) [[3], [11]]. Thus, for the reliable and economical manufacture of fuel cell materials, a process is needed that operates under the same conditions at lab-, pilot-, and large scale and is applicable for the production synthesis of a wide class of catalysts and electrodes.

Flame Spray Pyrolysis (FSP) is one of the promising flame-based synthesis technologies that could meet these requirements because the technique enables the rapid and continuous production of nano-powders in a single step [16]. The flame is fuelled by an organic solvent-based precursor solution that can contain several metal compounds and is atomized and combusted yielding product nanoparticles within milliseconds. The high temperature environment of the flame induces direct calcination and purification from organic or volatile contaminants [[16], [19]]. This *in-situ* way of synthesizing typically crystalline nanomaterials at high temperatures eliminates the need for various conventional pre- and post-treatment

steps and serves as a potential platform for the cost-effective and scalable production of nanomaterials with uniform composition and well-defined structural features. FSP-made nanomaterials have already found application for instance in ceramics, photocatalysis, biomaterials, medicine, batteries, semiconductors and sensors [[20], [21], [22], [23], [24]]. The rising interest in flame aerosol synthesis of nanomaterials is primarily due to its flexibility, speed, and scalability in nature [16]. The inherently continuous process can be scaled up by maintaining the particle residence time in the high-temperature reaction zone. Gröhn et al. [19], for instance, have increased the production rate for zirconia nanoparticles up to about 500 g h^{-1} without significantly affecting the nanoparticle characteristics such as primary particle and agglomerate size, morphology and crystallinity. Also, pilot-scale FSP plants producing several kg/h have been realized [25].

The versatility of the FSP method permits the synthesis of numerous nanomaterials with different microstructures for various applications including energy-related ones by changing the precursor solutions accordingly. FSP as a rapid nanomaterial synthesis technique facilitates systematic optimization of materials by variation of experimental conditions and geometric arrangements that govern flame characteristics and the particle residence time, such as precursor concentration, gas and precursor flow rates, quench and particle deposition distance or flame confinement. Thereby, laboratory-scale reactors generate nano-powders for each condition as quickly as a few minutes and as much as a several hundred milligrams. These features are the main advantages for the development of novel nanomaterials for fuel cell components, where expensive PGM and rare earth elements are used. Small batches for cost-effective screening and material optimization are obtained readily and the upscaling to a continuous process is comparably easy to implement. Consequently, substantial consumption of expensive resources can be avoided.

Until now, most publications on FSP for fuel cell applications focused only on material synthesis and lack electrochemical performance evaluation, especially for SOCs. This lack and the scarce use of FSP in the development next generation fuel cell materials may be caused by the missing link between FSP and fuel cell researchers. Therefore, the purpose of this review is (i) to provide a comprehensive view of recent progress in the synthesis and direct deposition of flame-made electrocatalysts for electrode/electrolyte components of PEMFC and SOC devices and (ii) to create awareness and bring researchers from FSP and fuel cell technologies close together. At first, this review will introduce and briefly discuss FSP techniques.

Then physicochemical and electrochemical properties of flame-made nanomaterials and films are addressed as well as fuel cell performance, if available. The basics of science and technology of flame synthesis, FSP and fuel cells are not covered in detail, though. Readers interested in further information on flame synthesis techniques are referred for instance to reviews by Koirala et al., Schimmoeller et al. or Teoh et al. [[16], [26], [27]]. Also, the review focuses on classical FSP techniques, i.e. liquid-fed spray flames where the precursor solution provides a substantial part of the combustion enthalpy [[28], [29]]. Related methods such as solid-fed sprays [30] or spray pyrolysis with extrinsic heating by a gaseous flame (so-called “flame-assisted spray pyrolysis” [[31], [32]]) or a furnace are not covered. Finally, a perspective on the future opportunities offered by the FSP technology for the development of sustainable fuel cells is provided and the possibility to boost the development of new generation materials for fuel cell applications is highlighted.

2. FSP Operation

A liquid-fed FSP set-up with various potential configurations is shown in Fig. 2. The metal-containing liquid or solid starting materials (precursors) are usually diluted with or dissolved in organic solvents to the desired stoichiometry. This precursor solution is metered to a spray nozzle, e.g. with syringe or continuous pumps and dispersed into fine droplets, typically using a twin-fluid atomizer. Oxygen or air are the standard dispersion gases, though other gases can be used as well. The spray is ignited and stabilized by a concentric pilot flame (blue in Fig. 2) based on methane or other gaseous fuels and oxygen. This spray flame actually constitutes the reactor (yellowish orange) in which particle formation and growth take place. The precursor solution thereby provides the majority of the total combustion enthalpy of the system.

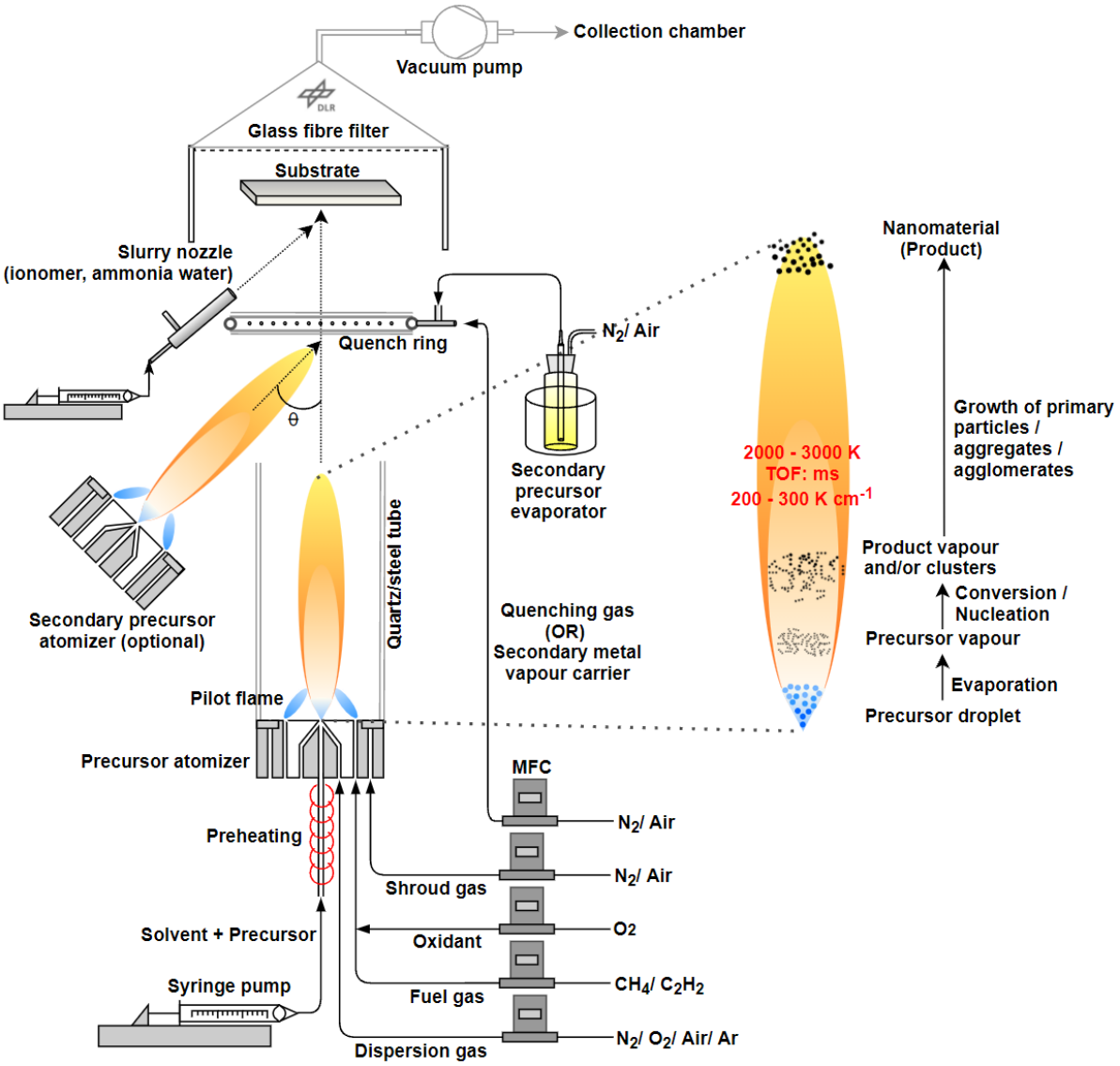

Fig. 2: Sketch of an FSP set-up, summarising various FSP techniques for powder production and thin-film deposition.

Inorganic or organic metal salts like nitrates, acetates or 2-ethylhexanoates along with metalorganic compounds like acetylacetonates or alkoxides are the commonly used precursors that are soluble in organic solvents such as xylene ($\Delta_c H^o_{298}$ = -4550 kJ mol^{-1}) and ethanol (-1376 kJ mol^{-1}). Also, non-volatile materials can thus be used as precursors in FSP making it more versatile and cheaper than other gas-phase synthesis processes that rely on starting materials with high vapour pressures [33]. Occasionally, liquified propane (-2219 kJ mol^{-1}) and acetone (-1772 kJ mol^{-1}) are added to the main solvents for better control of the atomization, the heat of combustion, and the flame temperatures [34]. Additionally, preheating of the

precursor solution containing such high equilibrium vapour pressure solvents helps to form ultra-fine droplets by increasing the pressure before atomization [34].

If an appropriate precursor solution is chosen [35], the spray droplets evaporate or undergo micro-explosions [[36], [37]] yielding precursor vapour that rapidly reacts to product molecules or small clusters [16]. FSP is a bottom-up process, i.e. particles primarily grow by coagulation and sintering. In the high temperature zone of the flame where sintering is rapid, particles fully fuse (coalesce) after collisions or form aggregates with sinter-bridges between primary particles. In zones of lower temperatures, sintering ceases while coagulation continues leading to the formation of agglomerates of primary particles and/or aggregates. With decreasing particle number concentration, coagulation slows down as well. The temperature, velocity and concentration profiles in the flame reactor along with the O_2 partial pressure govern particle growth and the structural and functional characteristics of the product nanoparticles [27].

In the standard configuration, FSP is operated in the open atmosphere or in systems with abundant oxygen for synthesizing oxide materials (*e.g.,* CeO_2, and perovskites). Depending on the precursor composition, the flame temperature at the reaction core can reach up to 3000 °C followed by rapid cooling with high temperature gradients of several hundred K cm^{-1}, induced by entrainment of surrounding air [27]. Almost all studies focussing on flame synthesis of fuel cell materials have employed this standard configuration.

Recent advancement in FSP techniques:

Shielding the flame from the atmosphere with a tube enclosure and introducing a shroud gas allows to control the O_2 partial pressure and therefore the oxidizing or reducing strength during particle synthesis [38]. Grass and Stark et al. [39], for instance, even produced metallic cobalt nanoparticles by reducing flame spray synthesis. Such conditions would be favourable, for producing non-oxide catalysts (*e.g.,* Pt/C, metal, and Metal-Nitrogen-Carbon (M-N-C) catalysts), but to the best of our knowledge, have not yet been explored for fuel cell materials apart from one study on Pt/C [40]. A tube enclosure further allows to modify the temperature profile and particle residence time by inducing recirculation which can be exploited to attain certain crystalline phases or larger primary particle sizes, as has been shown for some battery materials [[41], [42]].

A different means of altering the temperature profile is the introduction of a quench gas through a height-adjustable thermal quench ring – a stainless steel ring with numerous tiny jet nozzles placed in or downstream the flame that allows to rapidly freeze particle growth at cooling rates of up to 500 K cm^{-1} [43]. Thereby, the primary particle size can be reduced [43] and the formation of metastable compounds can be promoted [44]. For instance, Suffner et al. [45] achieved a metastable YSZ-Al_2O_3, where Al^{3+} cations have been incorporated into YSZ nano-particles at levels above the solubility limits. The authors claimed that the formation of metastable phases indicates nearly simultaneous nucleation of all three precursors - ZrO_2, Y_2O_3, and Al_2O_3 - from the vapour phase.

Teleki et al. [[46], [47]] and Sotiriou et al. [20] have used such a quench ring to introduce a secondary precursor in vapour form to *in-situ* encapsulate FSP-made titania and silver core catalysts with silica. Here, N_2 used as vapour carrier was also acting as quenching gas and assisted in preventing excess sintering of catalyst nanoparticles. Also, these techniques have not yet been explored for the production of advanced fuel cell materials.

Instead of using a quench ring for secondary metal vapour introduction, multiple FSP reactors can be combined (*e.g.,* dual-nozzle FSP) to co-precipitate - rather than sequentially precipitate - multi-component particles with controllable phase segregation [[27], [48]]. The technique enables independent control over particles synthesized in each flame, and circumvents the need for multiple FSP units and post-synthesis mixing steps to develop multi-component particles that need distinct fabrication conditions such as temperature [40]. Moreover, the flexibility to introduce an array of nozzles could also ease production scale-up to meet commercial volume.

The synthesized nanoparticles are either collected as a dry nano-powder on filters (glass or PTFE fibre discs for small batches or bag-house filters for continuous production) or by electrostatic precipitators. Particles can also be directly deposited as a film on a substrate [[49], [50]]. Also, the integration of a liquid dispersion step into the FSP process chain has been proposed to yield wet colloidal dispersions as products [51]. For direct deposition, the substrate is placed at an optimal height - stand-off distance - from the atomizer to avoid direct contact with the high-temperature flame. Additionally, the substrate is typically water-cooled to dissipate the heat experienced by the front side of the substrate [52]. Cooling enables coating of temperature-sensitive substrates that are interesting for PEMFC component development. It

helps to prevent thermal shock to the substrate and to reduce the stand-off distance between atomizer and substrate for CCM manufacturing directly onto polymeric electrolyte membranes (e.g., Nafion®) or decal foils (e.g. PTFE). However, in some configurations the substrate was electrically heated to influence the film properties [53]. Furthermore, appropriate thermostatisation could help to prevent the condensation of water on the substrate or to induce and control sintering for improved conductivity and mechanical layer stability [54]. The direct deposition of nanostructured films by FSP has advantages over conventional techniques such as screen printing and spin coating, where the stabilization of powders with high specific surface area (SSA, >40 m^2 g^{-1}) is critical and limited by the paste viscosity and the solids loading [17]. Besides, FSP-based direct deposition methods do not require additives that are associated with conventional wet deposition processes. Typically, no additional drying cycles are required after deposition [55], the film stoichiometry can be controlled in real-time, and different *in-situ* characterizations methods may be implemented to control the process.

In summary, the range of FSP techniques and their combination offers ample opportunities for the development of advanced fuel cell materials, that have been hardly exploited so far.

3. Flame synthesis and deposition techniques for fuel cell applications

Even though flame-based synthesis techniques have been used for producing nanomaterials for more than two decades now, relatively few publications address the development of components for fuel cell applications using this technology. In *2000,* Hwang et al. [56], described fabrication of platinum-catalyst coated polymer electrolyte membranes for fuel cells by the combustion chemical vapour deposition (CCVD) technique developed by Hunt and co-workers [[49], [51], [56], [57]]. Since then research groups around the world have developed dedicated systems analogous or similar to flame spray synthesis to fabricate materials for SOC and PEMFC electrodes/electrolytes. These include flame aerosol synthesis (FAS) by Choi, Lee and co-workers [[14], [58]], reactive spray deposition technique (RSDT) by the group of Maric [[13], [34], [53], [55], [59], [60], [61], [62], [63], [64], [65], [66], [67], [68], [69], [70], [71], [72], [73], [74]], aerosol flame deposition (AFD) by Shin and co-workers [[15], [52], [75], [76], [77], [78], [79], [80]], flame spray deposition (FSD) by the teams of Graule and Gauckler [[17], [81], [82], [83], [84], [85], [86], [87], [88], [89], [90]], FSP by Pratsinis, Mädler and co-workers [[40], [91], [92], [93]], liquid-precursor high velocity oxygen fuel flame (LT-HVOF) by Liu and team [[30], [57], [94]] as well as others [[45], [95], [96], [97], [98],

[99], [100], [101], [102], [103], [104], [105]]. Features of some of these major flame synthesis systems are briefly explained below.

The CCVD process of Hunt and co-workers uses pressure- and heat-assisted liquid atomization concepts to form very fine droplets before exit through a specially designed Nanomiser® nozzle [57]. The ultra-fine mist is then carried by an oxygen stream to combust in an atmospheric pressure flame. The resulting materials were either coated on substrates with a roll-to-roll web stock coater or collected as nano-powder on a rotating drum and dispersed in an appropriate liquid to obtain colloids. Using the CCVD technique, Hunt and co-workers have synthesized and tested numerous materials/components including Pt coated membrane electrode assemblies (MEA), Pt/C electrodes [[49], [56]], porous lanthanum strontium manganite (LSM), $Sm_{0.5}Sr_{0.5}CoO_3$ (SSC) [57], and dense YSZ [51], gadolinium-doped ceria (GDC), and samarium-doped ceria (SDC) [57] electrolytes for fuel cells.

Pratsinis, Mädler and co-workers have pioneered the advancement and understanding of the FSP technology and its application in the industrial-scale production of nanomaterials. While the early focus was on catalysts for environmental applications and chemical synthesis, materials for fuel cells included carbon-supported Pt and oxide supported noble metal catalysts [[16], [40], [43], [91]]. They were produced using an FSP system with various configurations including single/multiple FSP nozzles, quartz tube enclosure, quench ring and secondary precursor evaporators - similar to the arrangement shown in Fig. 2.

RSDT also follows an atomization procedure similar to CCVD using a heated reactor vessel of temperatures up to 150 °C to take a precursor solution diluted with liquefied propane to the supercritical point (about 1000 psi) before it enters into the atomizer. Downstream a quenching ring and thus in a low-temperature zone, a set of the air-assisted secondary nozzles can be used to spray suspensions (*e.g.* slurries of the support particles and ionomer) to mix secondary droplets/nanoparticles with the flame-made particles in-flight before deposition on the substrate [[55], [61]]. On the other end, the substrate holder moves such that the RSDT flame traverses from top to bottom at a fixed rate (10-100 mm s^{-1}) in an uninterrupted loop. This set-up has enabled the fabrication of various oxides [13], precious [67] and non-precious metal catalysts [[70], [71]], core-shell structures [[61], [106]] and supported catalysts [60], and thin layers of porous electrodes [13], dense electrolyte [53], and metal/ceramic supports [[55], [61], [62]] for SOC and PEMFC components.

Choi and Lee et al. [[14], [58]], have also produced carbon-supported catalysts by FAS technique using a specially designed acetylene-air co-flow diffusion flame reactor as shown in Fig. 3. It consisted of a central tube surrounded by four additional concentric channels that enabled the injection of inert gases (shield gas) between carbon source and PGM precursors to separate the carbon and Pt formation zones and to ensure carbon agglomeration before mixing with Pt. The liquid precursor was not atomized by a nozzle but an ultrasonic nebulizer before being transported to the reactor with a carrier gas. Unlike in other flame synthesis methods, the enthalpy for precursor conversion primarily came from acetylene and not from the solvent.

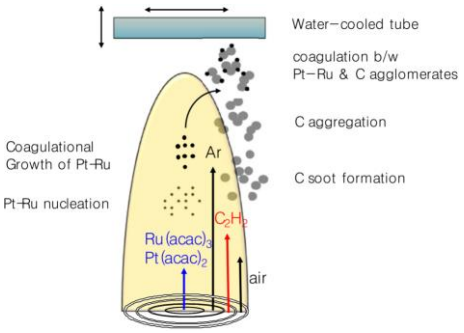

Fig. 3: Schematic of the FAS set up for synthesizing Pt1Ru1/C [58]. Adopted from Ref. [58] with permission from Elsevier and IOP Publishing Ltd.

Shin and co-researchers from Hanyang University, Korea, have deposited YSZ, GDC electrolytes, NiO/YSZ anode, and LSM cathode films for the intermediate temperature SOC system by AFD technique. AFD uses an oxygen-hydrogen torch made from four concentric quartz tubes to generate a flame. The centremost tube supplied fine droplets of precursor solution carried by a stream of argon and generated by an ultrasonic nebulizer similar to Choi et al. [14]. Fuel gas (H_2), shield gas (Ar), and oxygen flowed through the consecutive tubes, respectively. This burner design ensured a stable flame by creating a laminar flow of the gas mixture [[76], [80]]. Im et al. [15], have replaced the ultrasonic nebulizer with an electrostatically-assisted twin fluid atomizer, where electrical charging of droplets generated with the help of a high velocity Ar stream led to further breakdown yielding a very fine spray. This modification resulted in small primary particle sizes of 5-25 nm even for nitrate precursors and enabled linear control of the particle size by the applied electric field. Both ultrasonic and electrostatic atomization are suitable for research purposes but will have difficulty to compete with twin-fluid or pressure nozzles when it comes to continuous nanoparticle production at larger scale.

Though each of these flame-based processes has its design advantages in terms of atomization and flame generation, the core working principle, as described in section 2, remains the same for all. Therefore, and for the ease of readability, all these systems will be hereafter called either FSP or flame synthesis in general.

3.1. Flame synthesis for PEMFC applications

Catalytic conversion in PEMFCs takes place in the anodic and cathodic catalyst layer, which consist mainly of a supported electrocatalyst and an ionomer. Carbon-supported Pt and PGM-alloys are the state-of-the-art electrocatalysts for hydrogen oxidation reaction and oxygen reduction reaction (ORR) in PEMFCs (see Fig. 1). These nano-powders still show the greatest promise among all current catalytic structures but cannot completely cover the cost and durability targets required for fuel cell commercialization [8]. Generally, industrial-scale production of these catalysts is performed by impregnation of a metal precursor onto pre-prepared carbon supports followed by a reduction step in H_2 at high temperature or by reductive chemicals in wet chemical methods [107]. Catalysts made in this way often show broad particle size distribution, inhomogeneous catalyst distribution, and poor morphology [108]. The commonly used wet chemical methods require a large quantity of organic surfactants and solvents for yielding a few grams of catalysts [108]. In contrast to these techniques, FSP can continuously produce Pt-based catalyst nanoparticles from vapour in a flame and deposit them onto support structures (e.g., carbon and oxides) along with the flame synthesis. Table 1 shows a list of materials synthesized by flame synthesis for PEMFC applications.

Table 1: Flame-made nanomaterials and films for PEMFC applications.

Form	Material	Set-up	Metal precursor	Solvent	Particle size or film thickness	Morphology	Remarks	References
Powder	Pt on C	FSP	Acetylacetonate	Xylene or Ethanol	2.1±1.47 nm	Up to 12 wt.% Pt. Uniform Pt distribution without encapsulation and fewer Pt clusters	Dual-nozzle FSP, high carbon yield.	[40]
Powder	Pt on C	FAS	Acetylacetonate	Xylene	1.9±0.6 nm at 60 mm sampling height.	Up to 60 wt.% Pt. Uniform Pt distribution. No Pt cluster formation	82.5 m^2 mg_t^{-1} for 25 wt.%. Low carbon yield.	[14]

Powder	PtRu on C	FAS	Acetylacetonates	Xylene	1.9±0.6 nm at 80 mm sampling height	Well dispersed Pt-Ru particles of mole ratio 1:1.05. Amorphous-like Ru mixed into Pt lattice. Irregular size	72.9 m^2 mg^{-1} for 20 wt.%.	[58]
Powder	N-doped Pt on TiO_2	FSP	Chloroplatinic acid, Tetrabutyl titanate	Ethanol. ammonia water sprayed via slurry nozzle	Pt of 1.34±0.6 nm, TiO_2 of 10-25 nm	0.55 wt.% N interstitial doping. 3x increase in metallic Pt^o	Low aggregation of highly mobile Pt on TiO_2 stabilizes active sites upon heat treatment.	[98], [103]
Powder	Fe-N-C	RSDT	Iron (III) chloride and Cyanamide	Xylene, Methanol	10-30 nm of iron-rich nano-particles encapsulated within primary carbon	Mesoporous and uniform pore distribution. Layered graphitic structure,	Poor activity but low $\Delta E_{1/2}$ = 5 mV over 4000 cy. Chloride contamination.	[70]
Powder	Pt on CeO_2	RSDT	Acetylacetonate. CeO_2 introduced via slurry nozzle.	Xylene	Pt of 0.5-2 nm, CeO_2 of 8-30 nm	Pt evenly distributed on CeO_2	Low SSA and Pt loading.	[62]
Film with ionomer on Electrolyte or GDL	Pt on C	RSDT	Acetylacetonate	Acetone, Xylene (3:1 wt.%)	2.7±1 nm	bimodal distribution of pores with diameter 1.7-10 nm & 30-100 nm	62 m^2 mg^{-1} Covering C by ionomer prior to Pt impregnation may reduce carbon corrosion.	[[60], [65], [68]]
Film with PTFE binder on GDL	Pt on C	RSDT	Acetylacetonate	Acetone, Propane, Xylene	about 3 nm	Small and uniform pore size distribution at >0.5 binder/carbon ratio	44.4 m^2 mg^{-1}	[66]
Film with ionomer	PtRu on C	CCVD	-	-	1-5 nm	Aggregation, irregular size/shape.	-	[109]
Film without ionomer on GDL	PtRu	FAS	Acetylacetonates	Isooctane, Tetrahydrofuran	10.3±0.3 nm	Low Ru/Pt ratio. Crystalline Pt and amorphous Ru	60% higher ECSA than E-TEK10. No bulk alloying. partial surface alloying is insufficient to form homogeneous composition.	[95]
Film with ionomer on membrane	Pt-NbO_x/TiN	RSDT	Acetylacetonates, alkoxide	Methanol, xylene	1.6±1.0 nm	Uniform Pt dispersion and size distribution, porous	42.4 m^2 mg^{-1}	[110]

	and relatively uniform film

3.1.1 Electrocatalyst synthesis by flame synthesis

Researchers at ETH Zurich have synthesized Pt/C clusters (up to 12 wt.% Pt) with 220 m^2 g^{-1} SSA using a dual-nozzle FSP system [40]. The lower nozzle with a quartz tube enclosure was used for sub-stoichiometric combustion of a xylene aerosol and the formation of carbon nanoparticles in a controlled N_2 atmosphere. The upper nozzle generated Pt clusters that were mixed at an angle of 45° with the carbon support particles formed upstream. It should be highlighted that the carbon support particles are synthesized by this approach and are not just added in form of a slurry or dispersion. Thereby, the entire carbon-supported Pt catalyst could be prepared in one single process step. The applied method circumvents the catalytic effect of Pt on the combustion of carbon and the formation of carbon-embedded Pt particles. The size distribution of the Pt clusters with mean diameter of 2.1 nm had a geometric standard deviation close to the theoretical value of 1.46 for Brownian coagulation-coalescence in the free-molecular regime, indicating that Pt cluster formation (nucleation and coagulation) took place in the gas-phase before deposition on carbon support particles [40]. ECSA was not tested in this study. However, 10 wt.% Pt/C showed fair activity in the catalytic hydrogeneration of cyclohexane but still lower than that of 5 wt.% commercial Pt/C. This may indicate a need for improvement of Pt dispersion uniformity and removal of large Pt clusters.

Tight control on particle size and morphology is a must to avoid undesired particle coarsening that influences the catalytic activity. Roller et al. [68] have studied the influence of the oxidant content in their spray flame on Pt nanoparticle formation (without carbon support). It was found that increasing the oxygen flow rate at a constant fuel flow of 4 mL min^{-1} resulted in an increase in particle size and crystallinity as well as significantly reduced formation of very small and large Pt clusters. This was attributed to increasing flame turbulence leading to better disintegration and mixing of droplets, and more complete combustion in the reaction zone. Electrochemical activity tests of electrodes based on flame-made Pt showed that mass activity increased from 120 to 610 mA mg_{Pt}^{-1} and specific activity from 0.15 to 1.35 mA cm^{-2}, respectively for an increase in oxygen flow rate from 3.7 to 9.3 L min^{-1} (Fig. 4) [[68], [111]]. Though the increase in oxygen flow rate seems beneficial for a narrow Pt cluster size distribution, it may significantly reduce the carbon

yield in case of Pt/C synthesis. Therefore, a careful control of the oxygen partial pressure as well as the temperature field in and around the flame is crucial, along with a separation of reducing and oxidizing regions.

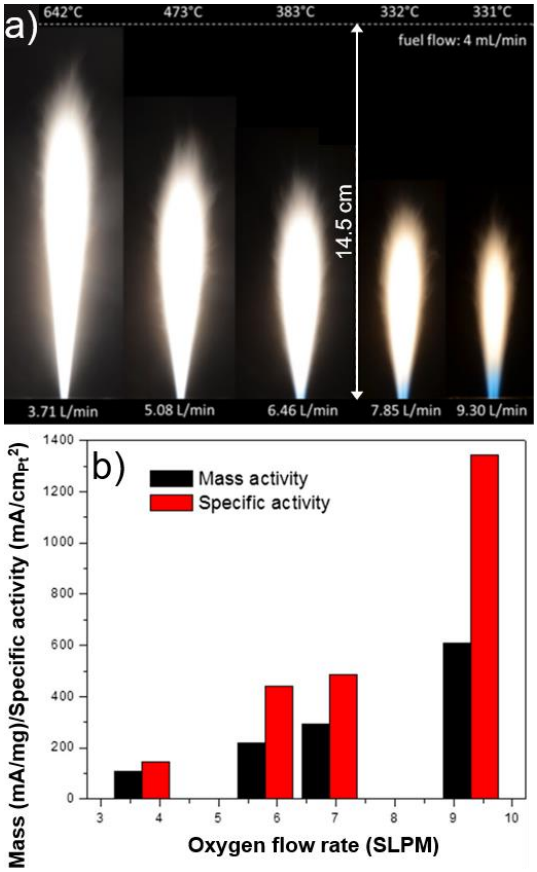

Fig. 4: (a) Flames with constant fuel flow of 4 mL min^{-1} and different oxygen flow rates of 3.7 to 9.3 L/min along with t_{gas} temperature at a fixed distance of 14.5 cm from the nozzle [34]. (b) Mass activity and specific activity of different flame-sprayed Pt electrodes with increasing oxygen flow rates [68]. Adopted from Ref. [[34], [68]] with permission from Springer Nature.

Choi et al. [14] produced Pt/C with 10-60 wt.% of Pt via a single nozzle FAS system, as described above. Pt(acac)$_2$ was dissolved in xylene to a concentration of 0.25 wt.% nebulized into 1-3 µm droplets in an ultrasonic atomizer with 30 psi compressed air and fed to a burner at 2.4 L min^{-1} through a heated tube. Nitrogen (shield gas), acetylene (source of heat and carbon), dry air (oxidant), and Ar (shroud gas or stabilizer) flowed through four concentric annuli at 2.0, 0.14, 1.4, and 20 L min^{-1}, respectively. Tight control over the mean size of metallic Pt particles as 1.8 nm (Fig. 5a) to 4.1 nm (Fig. 5b) and 6.2 nm (Fig. 5c) was

attained by simply varying the sampling heights from 60 mm to 85 mm and 120 mm. The surface dispersion/coverage of Pt on carbon support by adjusting the flow rate of acetylene (C_2H_2) or the concentration of Pt in xylene (Fig. 5e). A geometric standard deviation of the Pt size distribution close to 1.46 at 60 mm indicated Pt nucleation and growth by Brownian coagulation in the gas phase (Fig. 5d). Cyclic voltammetry (CV) of hydrogen adsorption/desorption using a 0.5 M H_2SO_4 electrolyte confirmed that the ECSA is higher than 74.9 $m^2\ g_{Pt}^{-1}$, more efficient than an equivalent commercial catalyst [14]. A reason for the high dispersion/coverage of Pt, and thereby good electrochemical performance, could be the separation of carbon inception from Pt formation. This was similar in the dual-nozzle study of Ernst et al. [40], where it prevented catalytic carbon burn-off and increased the carbon yield [40]. Further, a high flow rate of inert shield gas around the flame may have prevented Pt oxidation as indicated by Roller et al. [68] and improved the dispersion.

Using the FAS system, Lee et al. [58] produced 20 wt.% Pt-Ru/C particles (around 1:1 mole ratio of Pt:Ru) to circumvent the CO poisoning effect that inhibits the catalytic reaction of hydrogen in fuel cells. Pt-Ru particles had an average size of 1.9 ± 0.6 nm and were performance-tested for the methanol oxidation reaction against an equivalent commercial catalyst (E-TEK). The lower onset potential for methanol oxidation and the lower ratio of positive and negative scans in CV have demonstrated the benefits of the flame-made Pt-Ru/C [[58], [95]]. The ECSA was found to be 12% higher than for the E-TEK catalyst. This indicates a higher catalytic activity of the flame-made electrocatalyst in the application and thereby high reactivity toward the conversion of carbonaceous fuels. These results obtained for the flame made alloy catalyst promise that the flame synthesis process can be extended to develop a range of bulk and polycrystalline alloy electrocatalysts such as Pt_3-M, where 3d transition metals are used for alloy formation [108].

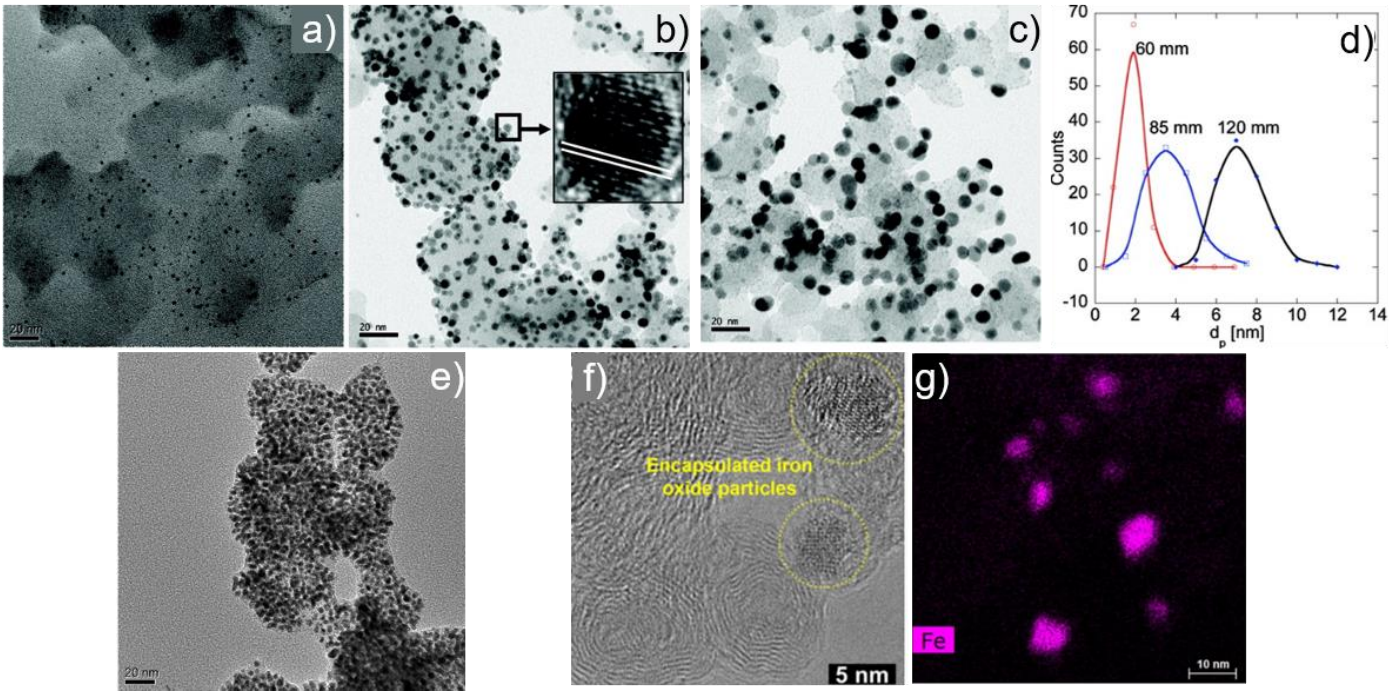

Fig. 5: (a-c) TEM images of flame-made Pt/C particles prepared from 0.25 wt.% of $Pt(acac)_2$ in xylene and 0.14 L min^{-1} acetylene flow collected at sampling heights of a) 60, b) 85, and c) 120 mm; (d) corresponding particle size distribution; (e) TEM image of 60 wt.% Pt/C obtained by lowering the acetylene flow rate to 0.12 L min^{-1} [14]. (f) High-resolution TEM image showing evidence of iron oxide nanoparticle encapsulation and (g) corresponding STEM EDX maps showing Fe distribution [70]. Adopted from ref. [[14], [70]] with permission from ACS and Springer Nature.

Transition metal oxides are discussed in literature as candidates for highly stable catalyst support materials, but the impact of the oxidic surface on platinum nucleation during catalyst deposition requires more complex synthesis methods like template-assisted routes to achieve highly active catalysts [112]. In FSP synthesis, it is possible to avoid heterogeneous nucleation/growth of noble metal catalysts directly on the support by separating the catalyst and support precursors using a dual nozzle FSP set up [103] (or using a co-flow diffusion flame reactor like Choi et al. [14]). Alternatively, rapid flame quenching can lead to homogeneous nucleation of the noble metal and could thus enable independent control of oxide support (e.g., TiO_2) and noble metal cluster characteristics. By quenching the flame at 2 - 12 cm above the burner, Schulz et al. [43] reported up to 40% smaller particle size (1.8 nm) and up to 25% higher Pt dispersion for 5-10 wt.% Pt on TiO_2compared to unquenched flames. Higher the quench gas flow rates and thus higher cooling rates and

Pt supersaturation in the flame led to more homogeneously-sized and uniformly-dispersed catalyst particles and less surface diffusion of Pt on TiO_2.

The reducibility of TiO_2 as a carrier (Pt/TiO_2) promotes catalytic activity in CO oxidation and can be of interest for CO-tolerant PEMFC catalysts [113]. However, the exothermic nature of the CO oxidation reaction causes sintering and aggregation by breaking/migrating Pt-O bonds during long-term use in PEMFCs [114]. A recent study by Bi et al. [98] describes *in-situ* interstitial N-doping in Ti-O-N and/or Ti-N-O structure by spraying an ammonia solution via a secondary nozzle placed downstream the flame. The N-doped Pt/TiO_2 exhibited Pt sizes ranging from 1-1.5 nm and showed high ECSA (Table 1) and thermal stability (ΔT_{100} = 10 °C) towards the complete conversion temperature of CO. This can be attributed to the formation of Pt-N bonds but was not confirmed with long-term catalytic stability studies. In a similar investigation using 26.6% $Pt\text{-}NbO_x$ on nano-sized TiN, Daudt et al. [110] have confirmed higher half-wave potential of 0.91 V and specific activity of 0.283 mA cm_{pt}^{-2} over commercial Pt/C for ORR in addition to the well-known catalytic stability of TiN support over carbon. Together, these results have confirmed high interaction between the thermally-synthesized catalysts and transition metal-based nano-supports, and thereby better catalytic and thermal stability.

Sub-stoichiometric titania nanoparticles (Magnéli phases, Ti_nO_{2n-1}, where $4 \leq n \leq 10$) are also very interesting support materials that exhibit conductivity comparable to graphite. Roller et al. [[55], [72]] tested commercially available Magnéli particles (Ebonex® - produced by high temperature reduction of TiO_2 in H_2 atmosphere and followed by several hours of ball milling) as support but observed poor performance of the MEA as compared to Pt/C-based samples. They attributed this to the low SSA of the support (about 10 m^2 g^{-1}), and therefore a low quantity of Nafion® for binding. The drawbacks of the rather large size of commercial particles could be overcome by producing sub-stoichiometric titania directly via flame synthesis [38]. Teleki and Pratsinis [115] obtained titanium suboxide particles (TiO_{2-x} with a significant fraction of Ti_9O_{17}) with SSA of up to 160 m^2 g^{-1} by controlling the burner to quenching ring distance in a co-flow diffusion flame reactor at reduced oxygen flow rate. The degree of sub-stoichiometry could also be fine-tuned by changing this distance and the precursor flow rate. Similar suboxides should be producible also by FSP as experiments with tube-enclosed spray flames at reduced oxygen partial pressure suggest [38]. To the best of our knowledge, flame-made Pt/Ti_nO_{2n-1} has not been synthesized yet but it is expected that this material can

be a highly stable and active catalyst system for PEMFC application if the electronic conductivity is appropriate.

PGM-free electrocatalysts are of high interest for PEMFC to overcome the cost barriers for commercialization. M-N-C catalysts using transition metals were demonstrated to be promising candidates for successful integration into PEMFCs [116]. Recently, an M-N-C-based electrocatalyst was synthesized for the first time using a modified FSP technique by Poozhikunnath et al. [70]. Fe-N-C was made by pyrolyzing a precursor of cyanamide and anhydrous $FeCl_3$ dissolved in a xylene-methanol mixture under oxygen-lean conditions, and a fuel equivalence ratio of 2.12 in a flame with a reaction zone temperature of about 1500 °C. Though a significant fraction of nanocrystalline graphitic carbon was found in the prepared material (Fig. 5f,g), the presence of inactive iron-rich phases and the low N/Fe atomic ratio resulted in only a few pyridinic M-N_x-coordinated active sites and few N-doped graphitic sites. Therefore, the ORR activity predominantly involved the transfer of two electrons with formation and reduction in a peroxide intermediate that lowered the activity. The presence of amorphous carbon also blocked access to active sites [71]. Given this unoptimized composition and process parameters, RDE measurements on the FSP-synthesized Fe-N-C showed a negligible reduction in the half-wave potential of 5 mV after 4000 potential cycles between 0.4 and 1.0 V in 0.1 M NaOH. It indicates higher stability than the equivalent wet-chemically synthesized Fe-N-C and commercial Pt/C [70]. Despite the observed low density of active sites, the superior stability of the FSP-made Fe-N-C catalyst is highly encouraging further investigation on flame synthesis of M-N-C as well as other PGM-free catalysts. The author suggested that the low volume density of active sites may be addressed by optimizing the Fe and N contents in the precursor, by exploring alternative nitrogen precursors, and by extending the length of the nitrogen-shielded reaction zone. In addition to this, the choice of a chloride iron precursor may have had adverse effects by inserting chlorine impurities.

3.1.2 Catalyst layer manufacturing by flame synthesis

In order to achieve cost targets for PEMFC commercialisation, substantial progress has been made to reduce the cathode Pt loading to about 0.1 mg_{Pt} cm^{-2}. A main limitation in reducing the Pt loading is performance loss at high-current density (>1.5 A cm^{-2}). This issue can be addressed through (i) the design of catalysts with high and stable Pt dispersion, (ii) developing methods to improve the interaction between Pt and ionomer (Nafion®), and (iii) the use of an optimum ratio of ionomer to carbon (I/C) because excess

ionomer can reduce the ECSA of the catalyst, the electronic conductivity and the pore volume of the catalyst layer (CL) and can impede the oxygen transport to the catalyst surface regardless of the catalyst loading [2]. Different CL fabrication methods may result in different optimum I/C values.

The FSP-based RSDT method holds promise as a one-step dry deposition process for low Pt loading by-passing traditional ink-based processing routes while independently controlling the Pt, ionomer, and support loading ratios in the final electrode in real-time [60]. A pre-mixture of commercially available carbon particles and ionomer was sprayed using air-assisted slurry nozzles into the relatively cold flame zone of the Pt-forming plume. The mixing zone was chosen in such a way that the temperature was high enough to establish interaction between Pt and support without decomposing the ionomer and before deposition onto a gas diffusion layer (GDL) or membrane [73]. Exemplary SEM cross-section images of flame-made CL (Pt/Vulcan with I/C = 0.5) on Nafion 211 are shown in Fig. 6a [65]. The process facilitated ionomer penetration into the carbon mesopores of up to 20 nm before mixing with Pt nanoparticles and thereby reduced the catalyst surface coverage by ionomer. Furthermore, it avoided localized ionomer agglomeration, and improved Pt distribution on the carbon surface [66]. The FSP-made low-temperature PEMFC electrodes with as low as 0.07 mg_{pt} cm^{-2} of Pt loading and I/C ratio of 0.3 showed a mass activity of 0.51 A mg_{pt}^{-1} for Pt/Ketjen black and 0.23 A mg_{pt}^{-1} for Pt/Vulcan XC-72R. In fuel cell operation, a current density of 1.4 A cm^{-2} at 0.6 V in H_2/O_2 operation at 80°C and 100% relative humidity (RH) and ECSA of 62 m^2 g_{pt}^{-1} was achieved, higher than the values of equivalent CL obtained by ink-based methods. The corresponding I-V curves are provided in Fig. 6b [65]. This indicates that the FSP-based techniques favour establishing triple-phase boundaries (TPB - contact between ionomer, catalyst and reactant) for better interaction between Pt, carbon, and ionomer so that less ionomer and less catalyst is required to achieve high proton conductivity and high catalyst activity.

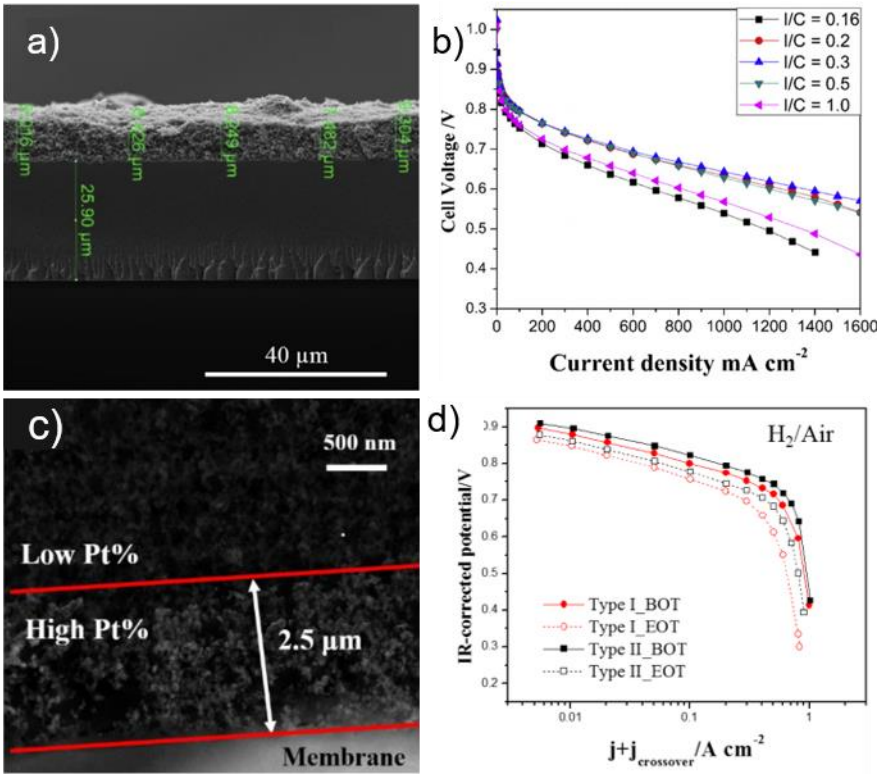

Fig. 6: (a) Cross-section image of FSP-made CL on Nafion 211. (b) I-V curves of RSDT-deposited CCMs with a Pt loading of 0.07 mg cm^{-2} and different I/C ratios, operated in H_2 (0.261 L min^{-1}) /O_2 (0.625 L min^{-1}) at 80 °C and 100% RH [65]. (c) HAADF STEM image of Type II cathode catalyst layer with low (40%) and high (60%) Pt loading regions. (d) Tafel plots comparing type I (gradient particle size) and type (gradient Pt loading) MEAs at the beginning-of-test (BOT) and end-of-test (EOT) in H_2/Air with 0.5/1.0 L min^{-1} and 100% RH [102]. Adopted from Ref. [[65], [102]] with permission from Elsevier.

Pt dissolution at the cathode and subsequent migration into the membrane are the major cause for catalyst degradation in PEMFC. In an effort to mitigated this issue Yu et al. [[101], [102]] fabricated cathode catalyst layers with gradients in Pt particle size (2 to 5 nm, Type I) and Pt loading (40% to 60%, Type II) by varying the flow rates of precursor, dispersion and quench gases during deposition. Yu et al. concluded that the end-of-test performance of the type II MEAs was high in comparison to the type I MEAs (Fig. 6c-d), and to the MEAs with uniform particle size (2 nm) and Pt loading in the cathodes [102].

The CL deposition conditions also influence the electrode surface morphology and, as a consequence, affect its specific and mass activity. For instance, Roller et al. [61] deposited Pd nanoparticles, that were

subsequently covered with a monolayer of Pt, on glassy carbon and GDL by FSP and varied the substrate temperature between 100 to 250 °C. Thereby, lower layer roughness was observed at higher temperature. Moreover, Pd nanoparticles had smoother surfaces and less sharp edges that are associated with low-coordination sites and easier oxidation. The electrode deposited at 250°C achieved a mass activity of 0.532 A mg_{pt}^{-1} and a peak power density of 0.93 W cm^{-2}, significantly higher than the 150°C sample. This further shows that FSP is a flexible technique for direct deposition of smooth surface layers.

Chakraborty et al. [95] reported that a FSP-produced and directly deposited PtRu (1:1 atomic ratio) thin layer on the GDL for methanol oxidation reaction at the anode of a DMFC outperformed a commercial PtRu/C with equal catalyst loading at up to about 1.6 times higher current density. This benefit could also be demonstrated at low current densities, i.e. just above the onset potential, where mass-transfer resistance due to the catalyst layer thickness is less significant. Similar performance was also measured for the MEA when the DMFC was producing power [95]. It is worth to note that the high performance of the flame-made PtRu arrives from its high ECSA and thus from the improved electrochemical efficiency of the catalyst, even though the specific metal surface area was about 10 times smaller than that of the commercial PtRu/C. Unlike a Pt-Ru powder made by Lee et al., [58], the Pt-Ru film prepared in this study had a low level of bulk alloying and results indicated the presence of amorphous Pt and Ru phases. This may be attributed to the abundance of air in the open FSP set-up and/or selection of comparatively low boiling point isooctane and tetrahydrofuran solvents by Chakraborty et al. [95] compared to xylene in Lee et al. [58]. The boiling point of the used isooctane deviates significantly from the melting point of the acetylacetonate precursors which may lead to inhomogeneous product powders [37]. Hence, it can be expected that further control over dispersion and morphology could yield higher performance.

3.2. Flame synthesis for SOC applications

Fabrication of various components for SOC using a single manufacturing technique is a challenging task as the microstructural and electrochemical requirements differ one from another. For instance, from a microstructural viewpoint, the electrolyte and interconnects must be highly dense to prohibit gas crossover and mixing whereas the anode and cathode should contain structurally organized pores to transport gas to the reaction sites. From an electrochemical viewpoint, electrolytes should be ionically conductive and electronically insulating, interconnects must be electronically conductive, and electrodes must be ionically

and electronically conductive. Nevertheless, all the components should possess comparable high thermal and chemical stability for better compatibility. The advantages of the FSP technique are that material synthesis and layer deposition can be combined in one single processing step and that both required layer structures, porous electrodes and dense electrolytes, can be produced with one device. For example, FSP produced highly porous LSM, SSC, $La_{0.6}Sr_{0.4}CoO_{3-\delta}$ (LSC) and $La_{0.6}Sr_{0.4}Co_{0.2}Fe_{0.8}O_{3-\delta}$ (LSCF) electrode films [[57], [80], [83]] while no porosity was observed in GDC and YSZ electrolyte films [[13], [84]] due to annealing, even though a strong increase in crystallographic density took place [83]. This shows that, the pore formation can be controlled by the selection of specific precursors and operation conditions. Table 2 shows the list of materials synthesized by flame synthesis for SOC applications.

Table 2: Flame-made nanomaterials and films for SOC applications.

Form	Material	Set-up	Metal precursor	Solvent	Particle size or film thickness	Morphology, purity	Remarks	References
				PEMFC				
Powder	YSZ Electrolyte	CCVD	Acetylacetonate, ethylhexanoate	-	~5 nm	Crystalline, Low agglomeration	Immediate dispersion in liquid reduce aggregation.	[51]
Powder	YSZ Electrolyte	AFD	Alkoxide, Nitrate	Ethanol, nitric acid	0.2–0.6 µm	Un-sintered, non-uniform	Ethanol may cause oxygen-deficient flame and micro-particle	[52]
Powder	ScSZ, ScCeSZ Electrolytes	FSS	Nitrates	DMF	8-20 nm	Crystalline, phase pure	10^{-2} S cm^{-1} at 600 °C	[81]
Powder	GDC Electrolyte	AFS	Nitrates	Methanol	5-25 nm & 100-200 nm	Bimodal size distribution, amorphous, phase segregation	10^{-2} S cm^{-1} at 700 °C	[15]
Powder	GDC Electrolyte	FSP	Nitrate, acetate	Ethanol	25 nm	Crystalline, loosely agglomerated	10^{-2} S cm^{-1} at 600 °C	[104]
Powder	Co-doped GDC Electrolyte	FSP	Carboxylates	Toluene	40 nm	Uniform, Spherical, crystalline	-	[90]
Powder	BZY Electrolyte	FSS	Carbonate, nitrate	Acetic acid, DMF, water	100 nm	Hollow, Ba nitrate phase segregation, phase pure after 1200 °C, dense after 1600 °C.	7.710^{-3} S cm^{-1} (as synthesised) and 4 10^{-3} S cm^{-1} (calcined) at 450 °C	[86]

Powder	Ni-doped BZY Electrolyte	FSS	Carbonate, nitrate	Acetic acid, DMF, water	10-200 nm	Large hollow particles, small phase segregated particles, amorphous	$3.8\ 10^{-3}$ S cm^{-1} (sintered) at 450 °C, Proton conductivity reduces with Ni inclusion but sintering temp. reduces up to 200 °C	[88]
Powder	LSM Cathode	AFD	Nitrates	Methanol	10-20 nm & few 200-300 nm	Phase pure, crystalline, aggregated, irregular shape	Rp 1.7 Ω cm^2 at 600 °C	[[79], [80]]
Powder	LSCF Cathode	FSS	Nitrates	DMF	5-10 nm	Homogenous, minor secondary phase	520 S cm^{-1} at around 400 °C	[82]
Powder	LSC Cathode	FSS	Nitrates	30% acetic acid in water	25-80 nm	Crystalline, less $(La,Sr)_2CoO_4$ secondary phase	2680 S cm^{-1} at 600 °C	[[17], [89]]
Powder	BSCF Cathode	FSS	Nitrates	DMF	10-20 nm	Aggregated, irregular shape, secondary carbonate phase.	56 S cm^{-1} at 500 °C	[82]
Powder	80NiO-20YSZ Anode	AFD	Nitrates	Methanol	10-500 nm	Bimodal size distribution, nano-crystals of NiO, large hallow particles with high YSZ fraction	Nitrates precipitation on droplet surface. 0.1 S cm^{-1} at 600 °C.	[77]
Powder	Nb-doped $(La,Sr)TiO_3$	FSS	Nitrates, chloride, acetylacetonate	DMF	35-45 nm	TiO2, Nb2O5 impurities, Sinterability improved with Nb doping.	226 S cm^{-1} at 900 °C	[87]
Film	YSZ Electrolyte	RSDT	Acetylacetonate, ethylhexanoate	Ethanol, Propane	5 µm grain size	Dense film achieved gradually on porous substrate	Ethanol-based oxygen-deficient flame cause temperature gradient	[[13], [81]]
Film	BZY	RSDT	Acetylacetonate, ethylhexanoate	Toluene, ethanol	2-5 µm film	Dense, non-uniform deposition, amorphous	-	[117]
Film	GDC Electrolyte	AFD	Nitrates	Methanol	5-20 nm	Porous, uniform. Dense after sintering at 1200 °C	10^{-2} S cm^{-1} at 800 °C	[[76], [78]]
Film	GDC Electrolyte	FSD	Nitrates	DMF or diethylene glycol butyl ether	-	Biphasic, amorphous, incomplete precursor evaporation	0.46 S cm^{-1} at 550 °C Large, dense, crack-free film after annealing	[[84], [85]]
Film	GDC DBL	RSDT	Alkoxides	Toluene	400 nm film	Dense, crystalline, phase pure	ASR 0.34 Ω cm^2 at 700 °C	[[13], [53]]

Film	LSC Cathode	FSD	Chlorides, Nitrates	DMF	38 nm film	Incomplete precursor evaporation, non-uniform, amorphous.	ASR of 0.96 Ω cm^2 at 600 °C	[83]
Film	LSCF	LT-HVOF	Nitrates	Alcohol-water	50-200 nm particles, 15-25 µm film	Rough, porous	Cathode Rp 0.15 Ω cm^2 at 600 °C	[94]
Film	SSC Cathode	RSDT	Acetylacetonate, ethylhexanoate	Ethanol, water, propane	2-3 µm film, 100-300 nm grains	Porous columnar microstructure, interconnected, inhomogeneous	656 mW/cm^2 at 600 °C	[13]
Film	SSC-SDC Cathode	CCVD	Nitrates	-	~50 nm grains	Highly porous, well adhered to electrolyte, crystalline	375 mW/cm^2 at 600 °C and 0.17 Ω cm^2	[57]
Film	70NiO-30YSZ Anode	AFD	Nitrates	Methanol	-	Porous, inhomogeneous	0.1 S cm^{-1} at 700 °C	[[75], [77]]
Film	NiO-SDC Anode	CCVD	Nitrates	Organic	~50 nm grains	Porous, crystalline, homogenous grains size	375 mW/cm^2 at 600 °C	[[57], [59]]
Film	Ni-BZY Anode	RSDT	Acetylacetonate, ethylhexanoate	Toluene, ethanol	5-10 µm film	30% Porosity, non-uniform, crystalline	ASR of 1 Ω cm^2 at 500 °C	[117]

3.2.1. Electrolytes prepared by flame synthesis

Stabilized zirconia and doped ceria are the two major electrolyte materials with a melting point of about 2700 °C and 2400 °C, respectively. They have to be sintered at high temperatures of 1400-1600 °C to obtain highly crystalline and dense (>95% of the theoretical density) layers. This may lead to undesirable interfacial reactions during co-sintering of electrolyte and electrodes and can also result in partial reduction of oxidic electrolytes (e.g., Ce^{4+} to Ce^{3+}), which contributes to an unwanted increase in the electronic conductivity of the electrolyte [59]. A potential solution to significantly reduce the sintering temperature of SOC components is to use nanostructured materials. In FSP, the short residence time in the flame with a high reaction temperature of 2000-3000 K generates crystalline nano-particles while steep cooling gradients allow particle deposition as a film on the substrate without co-sintering [59]. Another interesting aspect about particle synthesis by FSP is the possibility to work with two different particle formation mechanisms: gas-to-particle formation yielding nanosized products and droplet-to-particle formation leading to particles of some hundred

nanometres [33]. Im et al. [[15], [78]] synthesized different GDC powder batches with average particle sizes between 10 nm and 800 nm and a narrow size range by only fine-tuning the precursor concentration and the dispersion gas (O_2 and H_2) flow rate in an aerosol flame deposition setup. Films deposited on a Si wafer using particles with an average crystallite size of 14 nm showed dense microstructure with no open pores after sintering at 1200 °C for 10 h. Moreover, the ionic conductivity of the flame-made powders had reached 10^{-2} S cm^{-1} at 700 °C due to increase in the oxygen vacancies upon sintering at 1300 °C and above [15].

High production rate and utilization of cost-effective rare earth nitrates with high water content are promising routes for the commercialization of SOC technology. However, using such water-based precursor may cause bimodal particle size distribution and inhomogeneous elemental distribution. In FSP, this issue can be avoided by proper selection of metal precursors and solvents. For instance, Heel et al. [81] produced phase pure YSZ, $Sc_{0.2}Zr_{0.8}O_2$ (ScSZ), and $Sc_{0.2}Ce_{0.01}Zr_{0.79}O_2$ (ScCeSZ) nanocrystalline powders with SSA up to a 53 m^2 g^{-1} at production rates of about up to 260 g h^{-1} using an open flame. The authors have used water containing yttrium nitrate and zirconium alkoxide in combination with DMF as solvent and obtained dense nanoparticles with high thermal stability of up to 1000 °C. In a very similar study, You et al. [52] have used ethanol as solvent and obtained bimodal size distributions and hollow particles. The crystal water of the yttrium nitrate precursor may have reacted with the water-sensitive zirconium alkoxide in presence of ethanol leading to droplet shell formation [37]. Perhaps the use of DMF could have prevented the formation of large and hollow particles.

High temperature proton conducting ceramics based on Y- doped $BaZrO_3$ (BZY) are especially promising electrolytes for operation between 400°C and 600°C due to their high bulk conductivity and chemical stability. However, obtaining pure and crystalline $BaZr_{0.8}Y_{0.2}O_{3-\delta}$ is still challenging on conventionally-synthesized and heat treated BZY as Ba is highly volatile at high temperature [88]. Whereas, phase-pure BZY powder could be obtained by flame-synthesis and calcination at 1200 °C [86]. The author attribute this to the formation of Ba carbonate intermediate during heat treatment that aided in formation of pure BaZr0.8Y0.2O3-δ at low temperature. Upon sintering at 1600°C, the FSP-derived BZY showed enhanced grain growth and lower density of grain boundaries which resulted in low grain boundary resistance in the intermediate temperature range. The total conductivity measured at 450 °C was 7.7 mS cm^{-1}.

The high operating temperature of SOCs is the main concern that gives rise to its maintenance and safety issues as well as the subsequent decrease in power output. In an effort to reduce the operating temperatures, Karageorgakis et al. [[84], [85]] deposited dense and crack-free $Ce_{0.8}Gd_{0.2}O_{2-\delta}$ films on sapphire at as low as 200 °C and with a deposition rate as high as about 30 nm min^{-1} by flame spray pyrolyzing the nitrate-based precursors dissolved in DMF. The authors observed that two parameters are critical for their approach to obtain a crack-free and smooth surface: (i) the deposition temperature should be about 40-50 °C above the boiling point of the corresponding solvent and (ii) the carrier gas flow rates should be high enough to ensure limited residence time of the droplets in the hot zone. Deposition below the recommended temperature resulted in a cracked surface after annealing, whereas deposition above this temperature or using low carrier gas flow rates resulted in the formation of particles on the surface rather than films due to rapid evaporation of the solvent. Optimization of these deposition conditions yielded a homogeneous as-deposited film as observed with SEM (Fig. 7a). Further annealing at as low as 650 to 900 °C for 4 h (Fig. 7b) resulted in a dense and nanocrystalline microstructure with a fine grain size of 20-25 nm and a low surface roughness. The film annealed at 900 °C still contained a small fraction of amorphous phases that acted like a nanocomposite. This material demonstrated a maximum of hardness (11.5 ± 1.4 GPa) and an elastic modulus (310 ± 43 GPa) due to elastic strain, which is crucial for the microfabrication steps of the micro-SOFCs with free standing membranes [85]. Likewise, higher mechanical properties were also observed on flame-made YSZ films [118]. Unlike in typical flame aerosol procedures, the FSP, in these studies was operated in such a way that precursor-solvent droplets were not fully combusted when impinging on the substrate (liquid-to-solid conversion). This raises a question on chemical homogeneity. Nevertheless, the crystallographic density of 7.37 g cm^{-3} and the conductivity of 0.46 S m^{-1} at 550 °C obtained by the FSP-made and annealed (600 °C for 10 h) thin film (200 nm) were significantly higher than the one obtained by other high-temperature pyrolysis techniques [84]. This suggests a good electrochemical performance, but this was not reported, unfortunately.

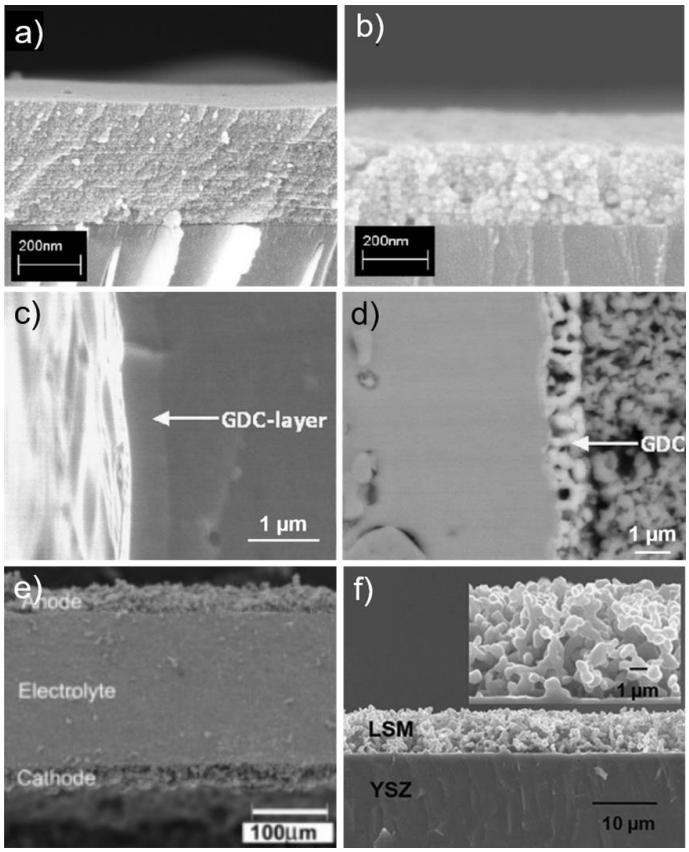

Fig. 7: (a-b) Cross sectional SEM images: for flame deposited GDC thin-films at 200 °C: (a) as-deposited and (b) annealed at 900 °C for 4 h [84]; (c-d) GDC as gas diffusion layer coated on YSZ electrolyte prepared by (c) FSP and (d) screen printing methods [53]; (e) the FSP-prepared NiO-SDC anode and SSC-SDC cathode; (f) LSM layers after sintering [80]. Adopted from Ref. [[53], [57], [80], [84]] with permission from Elsevier.

In order to make the fabrication of FSP-based films more suitable for industrial applications, it is important to eliminate post-deposition steps such as annealing. Maric et al. [13] investigated the possibility to grow uniform and dense (>99% density) YSZ (8 mol-% Y_2O_3) electrolyte directly on a 35% porous Ni-YSZ anode by increasing the substrate and flame temperatures at the deposition area to 950-1050 °C. Growing a dense film over a porous structure is challenging, however. The film deposited at 950 °C had a continuous layer of fine crystals, whereas the 1050 °C film showed large polycrystalline structures giving rise to porosity. They attribute this preferential growth to a higher thermal gradient in the growth direction, induced by the higher deposition temperature. Apparently, some parts of the porous substrate acted as individual growth centres and favoured preferential growth [13]. Maric et al. [13] proposed that this issue could be overcome

by using a two-layer deposition process - the first one with very low precursor concentration to form a dense base layer of about 100 nm on the porous electrode followed by a second dense electrolyte layer with higher precursor concentration to favour more homogeneous nucleation of growth centres on the substrate. These two layers can be realized continuously in a single run by using precursor solutions with different concentrations metered to a spray nozzle.

Similarly, Myles et al. [117] attempted to manufacture a metal-supported proton conducting SOFC by continuous deposition of porous electrodes and dense electrolyte structures without additional sintering steps through optimizing the heated substrate temperature and the distance between the flame tip to the substrate. In this preliminary study, flame-based layer by layer fabrication of porous Ni-BZY and LSCF electrode layers and dense BZY electrolyte layer was shown [74], however performance was not reported. Though the uniformity of the layer thickness and pore distribution in the electrodes were unsatisfactory, it can be expected that further optimization of precursor concentration and flow rates could enable progress towards the fabrication of a full proton conducting SOFC by flame-based deposition.

A ceria-based ultrathin diffusion barrier layer is often used at the interface between YSZ electrolyte and Sr-containing cathode to prevent solid state reaction during cell manufacturing and fuel cell operation. However, achieving a homogeneous, thin, fully crystalline, dense and continuous layer at a lower sintering temperature via conventional batch techniques (e.g., screen printing combined with sintering) is very challenging (Fig. 7d). Maric et al. [53], deposited such a GDC layer of 450 nm height on a 5 µm thick YSZ substrate at 1000 °C by the FSP technique. The GDC film shown in Fig. 7c appeared dense and homogeneous with no observable difference across the grain boundaries of the underlying YSZ, which reflects the quality of its morphology. The ohmic resistance of an anode-supported cell (5 cm x 5 cm) with FSP-made GDC layer (NiO/YSZ/GDC/LSC) was reduced by about 15% as compared to the cell with screen printed GDC, which should result in a significant increase in the cell performance.

3.2.2. Electrodes prepared by flame synthesis

Over the last two decades, the thickness of the electrolyte layer has been reduced substantially to improve the SOC performance. As a consequence, the ohmic resistance of the electrolyte has decreased and the overall cell losses are dominated by the polarization and transport losses of the electrochemical reactions

at the electrodes. Thus, it is important to reduce these losses of the electrodes, especially in case of anode-supported cells while referring to fuel cell operating mode. This can be achieved using films composed of nanoparticles, which provide high activity due to increased triple-phase boundary (TPB) density. Compared to conventional thin-film technology, FSP offers a reliable way to prepare such nano-porous films with a high deposition rate that ease the fabrication of films up to micrometre-scale thickness.

Preparation of fuel electrodes:

In anode-supported cells, Ni-YSZ and Ni-GDC are the widely used anode materials that show both electronic and O^{2-} ionic conductivity. Yoon et al. [[75], [77]] synthesized NiO-YSZ (60 mol% NiO – 40 mol% YSZ) powder and thin-films by the FSP method in air. The samples were composed mainly of YSZ and NiO catalytic particles of 10-20 nm in size. Further sintering at 600-900 °C for 2 h in 5% H_2 - 95% Ar reducing atmosphere (similar to anode operating conditions in SOC) converted NiO-YSZ into crystalline Ni-YSZ. This additional step ensured structural stability and increased electronic conductivity of the material in subsequent SOC operation in a H_2 atmosphere. It is worth emphasizing that the controlled reducing atmosphere can also be formed inside the FSP reactor itself by enclosing the reactor with a quartz tube. Thereby, the additional heat treatment step may be eliminated and direct deposition of porous anode films on a heated substrate could be realized. On the other hand, slightly reducing flame conditions can also be formed without a quartz tube by adjusting the precursor and oxygen flow. Using such a flame, Kazakevicius et al. [87] significantly reduced the formation of secondary phases (e.g., TiO_2 and Nb_2O_5) in as-synthesized Nb-doped (La,Sr)TiO_3 powder for the current-collecting layer in SOFC anodes by enabling suitable oxidation levels for Ti and Nb cations for their incorporation into a perovskite lattice structure. The electronic conductivity of the as-synthesized powder was not measured, however, the Nb-doped, flame-made and sintered (under reduced conditions) $La_{0.4}Sr_{0.412}Nb_{0.03}Ti_{0.97}O_{3-\delta}$ had the electronic conductivity of 226 S cm^{-1} at 900 °C.

Liu et al. [57] directly deposited a thin nanostructured NiO-SDC anode (70 wt.% Ni and 30 wt.% $Sm_{0.1}Ce_{0.9}O_{3-\delta}$) of 30 nm thickness on a 20 µm dense heated GDC electrolyte by FSP. The deposited film adhered well to the electrolyte layer (Fig. 7e) forming a highly interconnected porous structure with extremely low interfacial polarization resistances compared to those prepared by conventional techniques.

A power density of 375 mW cm^{-2} at 600 °C was measured with only little deterioration over 172 h of operation, indicating chemical and morphological robustness of the flame-made electrodes.

Preparation of oxygen electrodes:

Cathodes made of lanthanum manganite, ferrite or cobaltite materials showed high performance in terms of electronic conductivity and thermal and chemical compatibility with other SOC components. On the other hand, the selection of suitable synthesis methods also plays a major role in achieving a high level of porosity and a large ECSA for the ORR. Thereby, well-developed microstructures with increased TPB area and good adhesion between the cathode and the electrolyte can be realized in a reliable cost-effective manner.

Im et al. [80] deposited $La_{0.8}Sr_{0.2}MnO_{3\pm\delta}$ (LSM) cathode films onto 1 mm thick YSZ pellets of 94% density at about 500 nm min^{-1} deposition rate. The precursor was atomized and sprayed into a stable oxygen-hydrogen flame of about 1700 °C temperature. Based on electron microscopy analysis, the flame-prepared LSM powder had a bimodal particle size distribution with >98 wt.% primary nanoparticles of 10-20 nm and <2 wt.% of large particles of 200-300 nm, as is frequently observed when inorganic precursors are dissolved in alcohols [119]. Nevertheless, the overall SSA (77 m^2 g^{-1}) was higher than the LSM made by spray pyrolysis, combustion, wet chemical, or solid-state synthesis methods. Further, the LSM particles were noticeably smaller with less sintering when the growth was suppressed after particle formation by quenching. Fig. 7f shows an SEM image of a direct deposited LSM film after sintering at 1200 °C for 2 h [80]. The porous structure is deposited uniformly and seems to adhere well to the YSZ electrolyte.

Liu et al. [57] deposited a SSC-SDC (70:30 wt.%) composite material on a GDC electrolyte and investigated the significance of deposition temperature on morphology and performance. It was observed that deposition temperatures ≤1000 °C led to high interfacial resistance while temperatures ≥1400 °C resulted in an undesirably dense morphology with low interfacial polarization resistance (≤0.26 Ω cm^2). It appears that the temperatures between 1000 and 1400 °C provided favourable porous structures with low resistance. In another study, the performance of SOCs (NiO-YSZ/NiO-SDC/SDC) in fuel cell operation using SSC cathodes made by FSP against screen-printed SSC reference cells showed a 35% increase in peak power density and a 25% decrease in total polarization resistance at 600 °C [13]. The authors attribute this improved performance to the microstructure obtained by flame-based deposition that contains more open

pores, compared to the closed pore nature of the screen-printed and sintered cathodes which increases the surface exchange area of the cathodic material with the oxygen. These studies once again emphasize the simplicity of morphology control of the FSP-made components.

In addition to lowering the operation temperature of the cell, the development of economically viable and durable cell architectures such as metal-supported SOFCs is also crucial to enable their commercialization. However, metal supports may not be able to withstand high temperature heat treatments that are required to form desired electrode/electrolyte phases resulting in deformation and partial oxidation [120], especially the cathode. Zhang et al. [94] demonstrated FSP-deposition of LSCF (without any further heat treatment) on a ScSZ electrolyte- and Ni-ScSZ anode subsequently deposited on a porous steel support. The bonding onto the substrate was obtained by increasing the spray distance, and thus the residence time in the flame, in such a way that agglomerates melted partially and the deposited film remained porous upon growth. A symmetric cell (LSCF electrode |ScSZ electrolyte |LSCF electrode) fabricated using the optimized parameters showed cathodic R_p of 0.15 Ω cm^2 at 600 °C and the single cell (steel support |Ni-ScSZ anode |ScSZ electrolyte |LSCF cathode) showed R_p of 0.24 Ω cm^2 and peak power density of 0.65 W cm^{-2} at 600 °C that are promising values.

Though the morphology of powders and films can be well controlled in the flame atmosphere, one of the main disadvantages of using flame techniques is that the presence of carbon in the ligands and solvents may promote formation of metal carbonates during the cooling phase of the flame. Heel et al. [82] estimated a CO_2 partial pressure $P_{CO2,flame}$ of about 10^4-10^5 Pa during the combustion for their flame. The authors found a significant amount of secondary carbonate phases in FSP-made BSCF ($Ba_{0.5}Sr_{0.5}Co_{0.8}Fe_{0.2}O_{3-\delta}$), which is highly sensitive to CO_2 uptake. Consequently, the performance in terms of bulk conductivity was also reduced to 56 S cm^{-1} at 500 °C with an activation energy of 44.48 kJ mol^{-1}. Whereas, CO_2 insensitive LSCF ($La_{0.5}Sr_{0.5}Co_{0.8}Fe_{0.2}O_{3-\delta}$) had no secondary phases and showed high conductivity of 520 S cm^{-1} at 400 °C with an activation energy of 14.52 kJ mol^{-1} [82]. Carbonate formation may get severe when high surface area nanoparticles deposited on collection filters or on substrates are exposed to the CO_2 of the flame off-gas for prolonged times at temperatures that thermodynamically favour carbonates. The formation of carbonates may be reduced by passing the particles through these temperature zones quickly in addition

to minimizing the carbon content of the precursor solution and supporting flames, or by secondary heat treatments after synthesis.

$(La,Sr)_2CoO_4$ is the undesired secondary phase that reduces the ionic and the electronic conductivity of $La_{0.6}Sr_{0.4}CoO_{3-\delta}$ (LSC) cathodes. Heel et al. [[17], [89]] produced LSC powder and substantially decreased the fraction of (La,Sr)2CoO4 to about 10 wt.% by quenching the flame and optimizing the combustible solvent (acetic acid) to water ratio in the flame. A further reduction in secondary phase and homogeneous distribution of elements in the oxide structure may have been achieved with the selection of suitable combustible substances with high energy density instead of using a water-based precursor in this study. Nevertheless, the performance of the FSP-made LSC powder after heat-treatment at 700-800 °C was confirmed in comparison to screen-printed LSC films annealed at 700 °C for 4 h that showed semiconductor-like electronic bulk conductivity of about 2680 S cm^{-1} at 600 °C and 3600 S cm^{-1} at 400 °C in air.

It is a standard procedure in SOC that a certain amount of electrolyte powder is mixed with cathode powder in order to avoid the strong mismatch in the thermal expansion coefficient of LSC or LSM and that of electrolytes at the interface region. However, lower solid-state reactivity while mixing these two components and subsequent annealing at elevated temperature of up to 1000 °C is vital to evade formation of insulating secondary phases like $La_2Zr_2O_7$ and $SrZrO_3$ and to increase the TPB area [83]. Using FSP, Heel et al. [17] obtained nanoscale LSC powder with 29 m^2 g^{-1} SSA had outperformed and significantly lowered the formation of $La_2Zr_2O_7$ by about six times and $SrZrO_3$ by about twice compared to conventional spray-pyrolyzed sub-microscale LSC with 9 m^2 g^{-1} SSA while interacting with YSZ and $Sc_{0.20}Ce_{0.01}Zr_{0.79}O_{2-\delta}$ during annealing. This is surprising, as the nanoparticles were formed in an acetylene flame of about 3000K and exposed to a cooling rate in the order of 500 000 K s^{-1} that can cause non-stoichiometry with respect to oxygen and additional defect-related distortions [82]. The flame-made particles should thus contain a large number of reactive defect sites that would increase the percentage of such secondary phases. More research is needed to better understand the effect of flame synthesis parameters on the characteristics and performance of electrolyte-electrode interface layers.

4. Challenges and opportunities

The review shows that mainly simple oxide structures and perovskites with up to four cations have been produced successfully by FSP as powders or films until now, such as stabilized zirconia and ceria, Ni-YSZ, -SDC and -GDC, SSC-SDC, BSCF, LSM, LSC, LSCF, along with noble metal catalysts on carbon and oxide supports. For their synthesis, the standard FSP configuration operating in open air was employed in most cases. However, a number of new FSP techniques have been developed in recent years, as outlined in Section 2, which remain to be explored for the improvement of existing and the development of new advanced nanomaterials for fuel cells.

First, the possibility to influence the oxidizing/reducing conditions of the flame and to extend the particle growth time at high temperature by merely placing a simple tube enclosure around the FSP while controlling flow and composition of shroud gas (see Fig. 2) has gained too little attention, especially for fabrication of fuel cell materials. There are ample opportunities for the synthesis of certain metal nanoparticles, metal-carbon composites, or suboxides like TiOx, as indicated before. One may even explore the synthesis of oxynitrides that could find application in preparing catalysts for ultra-low Pt loaded PEMFC [121], by introducing appropriate nitrogen precursors. Tight control of the flame atmosphere toward pyrolysis in either Ar or NH_3 could also enable the synthesis of highly active M-N-C catalysts and the shift from two to four electron mechanism for ORR. In addition to this, alternative nitrogen-carrying precursors other than cyanamide and PANI with dicyandiamide should be explored. New pathways could even be explored by utilizing metal-organic frameworks including zeolitic imidazolates as precursors. Furthermore, controlled metal/nitrogen incorporation and pyrolysis via a fully enclosed FSP could yield powders with atomically dispersed elements; i.e. an increased density of MN_4 sites. Besides, enormous exertion on controlling the activity-stability trade-off along with particle size, porosity, graphitization and nitrogen-doping is still needed to achieve the targets for PGM-free catalysts by FSP.

Second, dual-nozzle FSP (see Fig. 2) should be explored further, e.g. for the synthesis of metal-metal oxides supported on carbon structures (e.g., $Pt/CeO_2/C$, $Pt/ZrO_2/C$ or Pt/FeO_x-CeO_2/C) that aid suppressing Pt oxide formation and promote ORR activity or can mitigate the formation of peroxides. A recent effort on the synthesis of a Pt/FeO_x-CeO_2 catalyst for preferential oxidation of CO (99.5%) below 90 °C demonstrates the opportunity for producing such multi-component nanomaterials in a single step process [122].

Third, the injection of a secondary precursor vapour downstream the FSP allows to in-situ deposit materials onto the surface of freshly-made nanoparticles (Fig. 2), yielding clusters, patchy coatings or full encapsulations. The technique was first demonstrated successfully for a TiO_2@SiO_2 photocatalyst at a production rate of about 30 g h^{-1} [47] and more recently with SnO_2-nanorods@TiO_2 for solar cell applications [106]. However, despite its capacity to generate more complex nanomaterials, it has not yet been explored for the fabrication of fuel cells. Potential candidates may be Ni@Pt, Pd@Pt or Cu@Pt that exhibit excellent ORR activity as compared to Pt/C for PEMFCs [123] or core-shell structures like LSC@CeO_2. Secondary precursor introduction could even be further expanded to the generation of soot flames based on carbon precursors (e.g., acetylene or evaporated aromatics) downstream the FSP to form carbon-supported core-shell structures such as Ni@Pt/C. The main challenges of secondary precursor introduction are the selection of an appropriate injection height with respect to temperature and, for formation of carbon black, control of oxygen concentration as well as of mixing between primary aerosol and secondary vapour. These factors govern the conversion of the secondary precursor, the point of nucleation in the gas phase or on the surface of core particles and the homogeneity of the product particles.

Forth, introduction of a slurry spray nozzle rather than a precursor vapour downstream the FSP allows for instance *in-situ* mixing of ionomer with catalyst and support particles [[60], [65]]. Followed by dry deposition on membrane or GDL, this provides great opportunity to modify CL architectures (e.g., SSA, pore size distribution, pore-volume, catalyst-ionomer-carbon ratios and film thickness). This unique combination of *in-situ* catalyst synthesis and flexibility in optimizing the film architecture may enable the fabrication of tailored films with ionomer phase segregated regions (hydrophobic and water-containing domains i.e. two-phase morphology) and composition. Thereby, increased surface exchange and TPB area and Pt utilization by targeting local inhomogeneities in fuel cell electrodes (e.g., water accumulation and oxygen depletion) may be achieved. Nevertheless, substantial process optimization is needed to achieve thin and uniform CL down to a few micrometres.

Fifth, the possibility to reach flame temperatures of up to 3000 K and ultra-fast quenching allows fabrication of complex materials and films that require high temperature processing for high phase purity, crystallinity and lattice parameters. For instance, flame synthesis of materials such as $SrNb_{0.1}Fe_{0.9}O_{3-\delta}$, and perovskite

proton conductors (e.g., $BaCe_{1-x-y}Zr_xY_yO_{3-\delta}$) that are very interesting for low temperature (400-500 °C) SOCs should be investigated.

Finally, the optimization of precursor chemistry is of paramount importance for achieving high quality nanomaterials for fuel cells as well as other applications. The drive towards low production costs inevitably leads to inorganic metal salts as raw materials, mostly nitrates. Their enticing price tag however comes with the downside of inhomogeneous product powders in terms of particle size and composition. Particle formation from nitrate-based precursor solutions in spray flames typically proceeds along two pathways: droplet-to-particle conversion yielding large sub-micrometre particles and gas-to-particle conversion yielding nanoparticles [33]. Product powders have a bimodal size distribution, which can lead to layer inhomogeneity with respect to porosity, thickness, integrity or mechanical stability. If multicomponent oxides are formed, differences in oxide vaporization rates can deplete the large particles of the more volatile species that would preferentially form nanoparticles by gas-to-particle conversion. Thus, layer inhomogeneities with respect to composition can develop as well. In order to prevent such inhomogeneities, the solvent mixture for the inorganic metal salts should be carefully designed, as outlined by Strobel and Pratsinis [124]. Particularly the presence of 2-ethylhexanoic acid was shown to prevent large particles by droplet-to-particle formation due to droplet disintegration by a series of micro-explosions in the flame [[36], [37]].

Nitrates, like many other metal salts, further have the disadvantage that they typically are hydrated, the level of which depends on the relative humidity of the surrounding atmosphere. As a consequence, their metal content varies and must be determined before precursor preparation. Otherwise, the correct stoichiometry of a multicomponent nanomaterial will not be achieved, leading to the formation of undesired secondary phases. Unfortunately, many publications do not report whether such a chemical analysis was carried out prior to FSP. Its omission, as well as the improper design of the solvent mixture, may explain why certain FSP-made fuel cell materials did not perform as expected or could have performed much better.

In summary, FSP is a facile and flexible platform that allows to combine multiple *in-situ* functionalities such as injection of secondary precursors, binders, additives, dopants, vapour coatings, quenching or direct deposition at various stages of nanomaterial and thin-film fabrication for PEMFC/SOC components. Thereby, it enables fabrication of complex supported catalysts, porous electrodes, dense electrolytes, and ultrathin DBL in single steps. The high synthesis temperature of the flame can potentially eliminate post-

heat treatments that are the major cause for surface crack formation, delamination and unavoidable batch processing. Though nanopowder manufacture by FSP is scalable, a key challenge remains the production of large-size components that could induce high residual thermal stress due to thermal expansion coefficient mismatch between neighbouring layers. This aspect is more critical in case of ceramic electrolyte-supported cell architectures that are vulnerable to thermal shock as compared to metal-supported ones. Nevertheless, overcoming these challenges, the successful deployment of FSP for producing all the nanomaterials and films for SOC/PEMFC applications would generate significant cost savings on energy and materials and promote the fuel cell market.

5. Concluding remarks

The suitability of FSP - where the flame is the reactor - as a potential platform for continuous synthesis of electrocatalysts and subsequent fabrication of active layers for PEMFC and SOC applications was assessed by analysis of literature. The ability of FSP to produce multicomponent nanomaterials at lab-scale up to industrial-scale cannot be matched by conventional methods. However, the literature lacks comparative studies regarding the fuel cell performance of materials made by FSP and by conventional methods, especially for SOCs. This comparison is required to demonstrate the full potential of FSP and to provide a proof-of-concept for the prepared catalysts and the catalyst layers. Although researchers have demonstrated the benefits of FSP in solving crucial fuel cell related issues through modifications in the experimental design, the recent advancements in FSP technology have hardly been exploited, yet. Establishing close interaction between the researchers advancing material applications, the flame aerosol scientists and fuel cell component manufacturers is crucial to bridge the gap between material research and fuel cell development.

Declaration of competing interest: The authors declare that they have no known competing financial interests or personal relationships that could have appeared to influence the work reported in this paper.

Acknowledgements: Permission for reproduced graphics have been obtained from the respective journals.

Author Contributions: Suriya Venkatesan: Conceptualization and writing - original draft preparation. Jens Mitzel and Karsten Wegner: conceptualization and writing - reviewing & editing. Remi Costa, Pawel

Gazdzicki and Kaspar Andreas Friedrich: writing - reviewing & editing. Jens Mitzel and Karsten Wegner contributed equally.

References

[1] Stambouli AB, Traversa E. Solid oxide fuel cells (SOFCs): a review of an environmentally clean and efficient source of energy. Renewable and Sustainable Energy Reviews. 2002;6:433-55

[2] Kongkanand A, Mathias MF. The Priority and Challenge of High-Power Performance of Low-Platinum Proton-Exchange Membrane Fuel Cells. J Phys Chem Lett. 2016;7:1127-37

[3] da Silva FS, de Souza TM. Novel materials for solid oxide fuel cell technologies: A literature review. International Journal of Hydrogen Energy. 2017;42:26020-36

[4] Hart D, Lehner F, Jones S, Lewis J. The Fuel Cell Industry Review 2019. http://www.fuelcellindustryreview.com/: E4tech; 2019. p. 1-51.

[5] Mitzel J, Zhang Q, Gazdzicki P, Friedrich KA. Review on mechanisms and recovery procedures for reversible performance losses in polymer electrolyte membrane fuel cells. Journal of Power Sources. 2021;488:229375.

[6] Jiao K, Xuan J, Du Q, Bao Z, Xie B, Wang B, et al. Designing the next generation of proton-exchange membrane fuel cells. Nature. 2021;595:361-9

[7] Fuel cells and hydrogen 2 joint undertaking (FCH 2 JU). https://www.fch.europa.eu/page/multi-annual-work-plan2018. p. 1-55.

[8] Banham D, Ye S. Current Status and Future Development of Catalyst Materials and Catalyst Layers for Proton Exchange Membrane Fuel Cells: An Industrial Perspective. ACS Energy Letters. 2017;2:629-38

[9] Olabi AG, Wilberforce T, Abdelkareem MA. Fuel cell application in the automotive industry and future perspective. Energy. 2021;214:118955.

[10] Singh M, Zappa D, Comini E. Solid oxide fuel cell: Decade of progress, future perspectives and challenges. International Journal of Hydrogen Energy. 2021;46:27643-74

[11] Abdalla AM, Hossain S, Azad AT, Petra PMI, Begum F, Eriksson SG, et al. Nanomaterials for solid oxide fuel cells: A review. Renewable and Sustainable Energy Reviews. 2018;82:353-68

[12] Niu G, Ruditskiy A, Vara M, Xia Y. Toward continuous and scalable production of colloidal nanocrystals by switching from batch to droplet reactors. Chem Soc Rev. 2015;44:5806-20

[13] Maric R, Roller J, Neagu R. Flame-Based Technologies and Reactive Spray Deposition Technology for Low-Temperature Solid Oxide Fuel Cells: Technical and Economic Aspects. Journal of Thermal Spray Technology. 2011;20:696-718

[14] Choi ID, Lee H, Shim YB, Lee D. A one-step continuous synthesis of carbon-supported Pt catalysts using a flame for the preparation of the fuel electrode. Langmuir. 2010;26:11212-6

[15] Im J, Park I, Shin D. Effect of atomization methods on the size and morphology of Gd0.1Ce0.9O2−δ powder synthesized by aerosol flame synthesis. Ceramics International. 2012;38:2051-8

[16] Koirala R, Pratsinis SE, Baiker A. Synthesis of catalytic materials in flames: opportunities and challenges. Chem Soc Rev. 2016;45:3053-68

[17] Heel A, Holtappels P, Graule T. On the synthesis and performance of flame-made nanoscale La0.6Sr0.4CoO3−δ and its influence on the application as an intermediate temperature solid oxide fuel cell cathode. Journal of Power Sources. 2010;195:6709-18

[18] Fan L, Zhu B, Su P-C, He C. Nanomaterials and technologies for low temperature solid oxide fuel cells: Recent advances, challenges and opportunities. Nano Energy. 2018;45:148-76

[19] Gröhn AJ, Pratsinis SE, Sánchez-Ferrer A, Mezzenga R, Wegner K. Scale-up of Nanoparticle Synthesis by Flame Spray Pyrolysis: The High-Temperature Particle Residence Time. Industrial & Engineering Chemistry Research. 2014;53:10734-42
[20] Sotiriou GA, Sannomiya T, Teleki A, Krumeich F, Vörös J, Pratsinis SE. Non-Toxic Dry-Coated Nanosilver for Plasmonic Biosensors. Advanced Functional Materials. 2010;20:4250-7
[21] Hamid NA, Wennig S, Hardt S, Heinzel A, Schulz C, Wiggers H. High-capacity cathodes for lithium-ion batteries from nanostructured LiFePO4 synthesized by highly-flexible and scalable flame spray pyrolysis. Journal of Power Sources. 2012;216:76-83
[22] Chen H, Mulmudi HK, Tricoli A. Flame spray pyrolysis for the one-step fabrication of transition metal oxide films: Recent progress in electrochemical and photoelectrochemical water splitting. Chinese Chemical Letters. 2020;31:601-4
[23] Pokhrel S, Madler L. Flame-made Particles for Sensors, Catalysis, and Energy Storage Applications. Energy Fuels. 2020;34:13209-24
[24] Liu S, Mohammadi MM, Swihart MT. Fundamentals and recent applications of catalyst synthesis using flame aerosol technology. Chemical Engineering Journal. 2021;405:126958.
[25] Wegner K, Schimmöller B, Thiebaut B, Fernandez C, Rao TN. Pilot plants for industrial NP production by FSP. KONA Powder and Particle Journal. 2011;29:251-65
[26] Schimmoeller B, Pratsinis SE, Baiker A. Flame Aerosol Synthesis of Metal Oxide Catalysts with Unprecedented Structural and Catalytic Properties. ChemCatChem. 2011;3:1234-56
[27] Teoh WY, Amal R, Madler L. Flame spray pyrolysis: An enabling technology for nanoparticles design and fabrication. Nanoscale. 2010;2:1324-47
[28] Bickmore CR, F. WK, Treadwell DR, Laine RM. Ultrafine spinel powders by LF-FSP of a Magnesium Aluminum Double Alkoxide. J Am Ceram Soc. 1996;79:1419-23
[29] Madler L, Kammler HK, Mueller R, Pratsinis SE. Controlled synthesis of nanostructured particles by flame spray pyrolysis. Journal of Aerosol Science. 2002;33:369-89
[30] Zhang S-L, Li C-X, Li C-J, Yang G-J, Liu M. Application of high velocity oxygen fuel flame (HVOF) spraying to fabrication of La0.8Sr0.2Ga0.8Mg0.2O3 electrolyte for solid oxide fuel cells. Journal of Power Sources. 2016;301:62-71
[31] Charojrochkul S, Choy KL, Steele BCH. Flame assisted vapour deposition of cathode for solid oxide fuel cells. 1. Microstructure control from processing parameters. Journal of the European Ceramic Society. 2004;24:2515-26
[32] Sansernnivet M, Laosiripojana N, Assabumrungrat S, Charojrochkul S. Fabrication of La0.8Sr0.2CrO3-based Perovskite Film via Flame-Assisted Vapor Deposition for H2 Production by Reforming. Chemical Vapor Deposition. 2010;16:311-21
[33] Strobel R, Pratsinis SE. Flame aerosol synthesis of smart nanostructured materials. Journal of Materials Chemistry. 2007;17:4743-56
[34] Roller JM, Maric R. A Study on Reactive Spray Deposition Technology Processing Parameters in the Context of Pt Nanoparticle Formation. Journal of Thermal Spray Technology. 2015;24:1529-41
[35] Rudin T, Wegner K, Pratsinis SE. Uniform nanoparticles by flame-assisted spray pyrolysis (FASP) of low cost precursors. J Nanopart Res. 2011;13:2715-25
[36] Li H, Pokhrel S, Schowalter M, Rosenauer A, Kiefer J, Madler L. The gas-phase formation of tin dioxide nanoparticles in single droplet combustion and flame spray pyrolysis. Combust Flame. 2020;215:389-400
[37] Rosebrock CD, Wriedt T, Mädler L, Wegner K. The role of microexplosions in flame spray synthesis for homogeneous nanopowders from low-cost metal precursors. AIChE Journal. 2016;62:381-91
[38] Kho YK, Teoh WY, Mädler L, Amal R. Dopant-free, polymorphic design of TiO2 nanocrystals by flame aerosol synthesis. Chemical Engineering Science. 2011;66:2409-16
[39] Grass RN, Stark WJ. Gas phase synthesis of fcc-cobalt nanoparticles. Journal of Materials Chemistry. 2006;16:1825-30

[40] Ernst FO, Büchel R, Strobel R, Pratsinis SE. One-Step Flame-Synthesis of Carbon-Embedded and -Supported Platinum Clusters. Chemistry of Materials. 2008;20:2117-23
[41] Waser O, Hess M, Güntner A, Novák P, Pratsinis SE. Size controlled CuO nanoparticles for Li-ion batteries. Journal of Power Sources. 2013;241:415-22
[42] Waser O, Brenner O, Groehn AJ, Pratsinis SE. Process Design for Size-Controlled Flame Spray Synthesis of Li4Ti5O12 and Electrochemical Performance. Chemical and Process Engineering. 2017;38:51-66
[43] Schulz H, Mädler L, Strobel R, Jossen R, Pratsinis SE, Johannessen T. Independent Control of Metal Cluster and Ceramic Particle Characteristics During One-step Synthesis of Pt/TiO2. Journal of Materials Research. 2011;20:2568-77
[44] Jodhani G. Flame Spray Pyrolysis Processing to Produce Metastable Phases of Metal Oxides. Juniper Online Journal Material Science. 2017;1:555557.
[45] Suffner J, Wang D, Kübel C, Hahn H. Metastable phase formation during flame spray pyrolysis of ZrO2(Y2O3)–Al2O3 nanoparticles. Scripta Materialia. 2011;64:781-4
[46] Teleki A, Buesser B, Heine MC, Krumeich F, Akhtar MK, Pratsinis SE. Role of Gas−Aerosol Mixing during in Situ Coating of Flame-Made Titania Particles. Industrial & Engineering Chemistry Research. 2008;48:85-92
[47] Teleki A, Heine MC, Krumeich F, Akhtar MK, Pratsinis SE. *In Situ* Coating of Flame-Made TiO_2 Particles with Nanothin SiO_2 Films. Langmuir. 2008;24:12553-8
[48] Strobel R, Mädler L, Piacentini M, Maciejewski M, Baiker A, Pratsinis SE. Two-Nozzle Flame Synthesis of Pt/Ba/Al_2O_3 for NO_x Storage. Chemistry of Materials. 2006;18:2532–7
[49] Hunt AT, Carter WB, Cochran JK. Combustion chemical vapor deposition: A novel thin-film deposition technique. Applied Physics Letters. 1993;63:266-8
[50] Mädler L, Roessler A, Pratsinis SE, Sahm T, Gurlo A, Barsan N, et al. Direct formation of highly porous gas-sensing films by in situ thermophoretic deposition of flame-made Pt/SnO2 nanoparticles. Sensors and Actuators B: Chemical. 2006;114:283-95
[51] Oljaca M, Xing Y, Lovelace C, Shanmugham S, Hunt AT. Flame synthesis of nanopowders via combustion chemical vapor deposition. Journal of Materials Science Letters. 2002;21:621 – 6
[52] You H, Cho K, Yoon Y, Im J, Shin D. Synthesis of yttria-stabilized zirconia film by Aerosol Flame Pyrolysis Deposition. Journal of Analytical and Applied Pyrolysis. 2008;81:14-9
[53] Maric R, Neagu R, Zhang-Steenwinkel Y, van Berkel FPF, Rietveld B. Reactive Spray Deposition Technology – An one-step deposition technique for Solid Oxide Fuel Cell barrier layers. Journal of Power Sources. 2010;195:8198-201
[54] Tricoli A, Graf M, Mayer F, Kuühne S, Hierlemann A, Pratsinis SE. Micropatterning Layers by Flame Aerosol Deposition-Annealing. Advanced Materials. 2008;20:3005-10
[55] Roller JM, Arellano-Jiménez MJ, Yu H, Jain R, Carter CB, Maric R. Catalyst nanoscale assembly from the vapor phase on corrosion resistant supports. Electrochimica Acta. 2013;107:632-55
[56] Hwang TJ, Shao H, Richards N, Schmitt J, Hunt A, Lin W-Y. Platinum-Catalyzed Polymer Electrolyte Membrane for Fuel Cells. MRS proceedings. 2000;575:239-46
[57] Liu Y, Zha S, Liu M. Novel Nanostructured Electrodes for Solid Oxide Fuel Cells Fabricated by Combustion Chemical Vapor Deposition (CVD). Advanced Materials. 2004;16:256-60
[58] Lee H, Kim TJ, Li C, Choi ID, Kim YT, Coker Z, et al. Flame aerosol synthesis of carbon-supported Pt–Ru catalysts for a fuel cell electrode. International Journal of Hydrogen Energy. 2014;39:14416-20
[59] Maric R, Seward S, Faguy PW, Oljaca M. Electrolyte Materials for Intermediate Temperature Fuel Cells Produced via Combustion Chemical Vapor Condensation. Electrochemical and Solid-State Letters. 2003;6:A91-A5
[60] Roller J, Neagu R, Orfino F, Maric R. Supported and unsupported platinum catalysts prepared by a one-step dry deposition method and their oxygen reduction reactivity in acidic media. Journal of Materials Science. 2012;47:4604-11

[61] Roller J, Yu H, Vukmirovic MB, Bliznakov S, Kotula PG, Carter CB, et al. Flame-Based Synthesis of Core-Shell Structures Using Pd-Ru and Pd Cores. Electrochimica Acta. 2014;138:341-52
[62] Jain R, Maric R. Synthesis of nano-Pt onto ceria support as catalyst for water–gas shift reaction by Reactive Spray Deposition Technology. Applied Catalysis A: General. 2014;475:461-8
[63] Hu G, Neagu R, Wang Q, Zhang Z, Li G, Zheng Y. Mathematical Modelling of Flow and Heat/Mass Transfer During Reactive Spraying Deposition Technology (RSDT) Process for High Temperature Fuel Cells. Engineering Applications of Computational Fluid Mechanics. 2014;6:134-43
[64] Myles TD, Kim S, Maric R, Mustain WE. Application of a Coated Film Catalyst Layer Model to a High Temperature Polymer Electrolyte Membrane Fuel Cell with Low Catalyst Loading Produced by Reactive Spray Deposition Technology. Catalysts. 2015;5:1673-91
[65] Yu H, Roller JM, Mustain WE, Maric R. Influence of the ionomer/carbon ratio for low-Pt loading catalyst layer prepared by reactive spray deposition technology. Journal of Power Sources. 2015;283:84-94
[66] Kim S, Myles TD, Kunz HR, Kwak D, Wang Y, Maric R. The effect of binder content on the performance of a high temperature polymer electrolyte membrane fuel cell produced with reactive spray deposition technology. Electrochimica Acta. 2015;177:190-200
[67] Ayers KE, Renner JN, Danilovic N, Wang JX, Zhang Y, Maric R, et al. Pathways to ultra-low platinum group metal catalyst loading in proton exchange membrane electrolyzers. Catalysis Today. 2016;262:121-32
[68] Roller JM, Kim S, Kwak T, Yu H, Maric R. A study on the effect of selected process parameters in a jet diffusion flame for Pt nanoparticle formation. Journal of Materials Science. 2017;52:9391-409
[69] Yu H, Danilovic N, Wang Y, Willis W, Poozhikunnath A, Bonville L, et al. Nano-size IrOx catalyst of high activity and stability in PEM water electrolyzer with ultra-low iridium loading. Applied Catalysis B: Environmental. 2018;239:133-46
[70] Poozhikunnath A, Yu H, Bonville L, Myles T, Maric R. Characterization and evaluation of Fe–N–C electrocatalysts for oxygen reduction directly synthesized by reactive spray deposition technology. Journal of Materials Science. 2019;55:1673-91
[71] Poozhikunnath A. Characterization and Optimization of Carbon Based Electrocatalysts and Supports for Fuel Cell Applications [Doctoral Dissertations]. https://opencommons.uconn.edu/dissertations/23502019.
[72] Roller J, Renner J, Yu H, Capuano C, Kwak T, Wang Y, et al. Flame-based processing as a practical approach for manufacturing hydrogen evolution electrodes. Journal of Power Sources. 2014;271:366-76
[73] Yu H, Roller JM, Kim S, Wang Y, Kwak D, Maric R. One-Step Deposition of Catalyst Layers for High Temperature Proton Exchange Membrane Fuel Cells (PEMFC). Journal of The Electrochemical Society. 2014;161:F622-F7
[74] Ouimet RJ, Gado AM, Bliznakov S, Bonville LJ, Maric R. Advanced electrodes for electrochemical energy storage and conversion devices fabricated by reactive spray deposition technology. Electrochemistry Communications. 2021;133
[75] Yoon Y, Im J, You H, Shin D. Fabrication of NiO/YSZ anode for solid oxide fuel cells by aerosol flame deposition. Journal of the European Ceramic Society. 2007;27:4257-60
[76] Im JM, You HJ, Yoon YS, Shin DW. Synthesis of nano-sized gadolinia doped ceria powder by aerosol flame deposition. Journal of the European Ceramic Society. 2007;27:3671-5
[77] Yoon YS, Im JM, Shin DW. Microstructure and electrical conductivity of NiO–YSZ nano-powder synthesized by aerosol flame deposition. Ceramics International. 2008;34:873-6
[78] Im JM, You HJ, Yoon YS, Shin DW. Synthesis of nano-crystalline Gd0.1Ce0.9O2−x for IT-SOFC by aerosol flame deposition. Ceramics International. 2008;34:877-81
[79] Jung YG, Choi J, Yoon Y, Shin D. Characterization of La(0.8)Sr(0.2)MnO(3 +/-delta) nanopowders synthesized by aerosol flame synthesis for SOFC cathode. J Nanosci Nanotechnol. 2011;11:7475-8

[80] Im J, Park I, Shin D. Preparation of nano-crystalline strontium-doped lanthanum manganate (LSM) powder and porous film by aerosol flame deposition. Ceramics International. 2014;40:5567-73
[81] Heel A, Vital A, Holtappels P, Graule T. Flame spray synthesis and characterisation of stabilised ZrO2 and CeO2 electrolyte nanopowders for SOFC applications at intermediate temperatures. Journal of Electroceramics. 2009;22:40-6
[82] Heel A, Holtappels P, Hug P, Graule T. Flame Spray Synthesis of Nanoscale La0.6Sr0.4Co0.2Fe0.8O3-δ and Ba0.5Sr0.5Co0.8Fe0.2O3-δ as Cathode Materials for Intermediate Temperature Solid Oxide Fuel Cells. Fuel Cells. 2010;10:419-32
[83] Karageorgakis NI, Heel A, Bieberle-Hütter A, Rupp JLM, Graule T, Gauckler LJ. Flame spray deposition of La0.6Sr0.4CoO3−δ thin films: Microstructural characterization, electrochemical performance and degradation. Journal of Power Sources. 2010;195:8152-61
[84] Karageorgakis NI, Heel A, Graule T, Gauckler LJ. Flame spray deposition of nanocrystalline dense Ce0.8Gd0.2O2−δ thin films: Deposition mechanism and microstructural characterization. Solid State Ionics. 2011;192:464-71
[85] Karageorgakis NI, Heel A, Rupp JLM, Aguirre MH, Graule T, Gauckler LJ. Properties of Flame Sprayed Ce0.8Gd0.2O1.9-δ Electrolyte Thin Films. Advanced Functional Materials. 2011;21:532-9
[86] Bozza F, Arroyo Y, Graule T. Flame Spray Synthesis of BaZr0.8Y0.2O3-δElectrolyte Nanopowders for Intermediate Temperature Proton Conducting Fuel Cells. Fuel Cells. 2015;15:588-94
[87] Kazakevičius E, Tsekouras G, Michalow-Mauke KA, Kazlauskas S, Graule T. Electronic Conductivity Enhancement of (La,Sr)TiO3with Nb-Doping on B-Site. Fuel Cells. 2014;14:954-60
[88] Bozza F, Bator K, Kubiak WW, Graule T. Effects of Ni doping on the sintering and electrical properties of BaZr 0.8 Y 0.2 O 3− δ proton conducting electrolyte prepared by Flame Spray Synthesis. Journal of the European Ceramic Society. 2016;36:101-7
[89] Prestat M, Morandi A, Heel A, Holzer L, Holtappels P, Graule TJ. Effect of graphite pore former on oxygen electrodes prepared with La0.6Sr0.4CoO3− nanoparticles. Electrochemistry Communications. 2010;12:292-5
[90] Jud E, Gauckler L, Halim S, Stark W. Sintering Behavior of In Situ Cobalt Oxide-Doped Cerium-Gadolinium Oxide Prepared by Flame Spray Pyrolysis. Journal of the American Ceramic Society. 2006;0:060623005134001-???
[91] Strobel BR, Pratsinis SE. Flame Synthesis of Supported Platinum Group Metals for Catalysis and Sensors. Platinum Metals Review. 2009;53:11-20
[92] Mädler L, Stark WJ, Pratsinis SE. Flame-made Ceria Nanoparticles. Journal of Materials Research. 2002;17:1356-62
[93] Buergler B, Siegrist M, Gauckler L. Single chamber solid oxide fuel cells with integrated current-collectors. Solid State Ionics. 2005;176:1717-22
[94] Zhang S-L, Yu H-X, Li C-X, Lai SY, Li C-J, Yang G-J, et al. Thermally sprayed high-performance porous metal-supported solid oxide fuel cells with nanostructured La0.6Sr0.4Co0.2Fe0.8O3−δ cathodes. Journal of Materials Chemistry A. 2016;4:7461-8
[95] Chakraborty D, Bischoff H, Chorkendorff I, Johannessen T. Mixed Phase Pt-Ru Catalyst for Direct Methanol Fuel Cell Anode by Flame Aerosol Synthesis. Journal of the Electrochemical Society. 2005;152:A2357-A63
[96] Dahl PI, Colmenares LC, Barnett AO, Lomas S, Vullum PE, Kvello JH, et al. Flame spray pyrolysis of tin oxide-based Pt catalysts for PEM fuel cell applications. MRS Advances. 2017;2:1505-10
[97] Dahl PI, Thomassen MS, Colmenares LC, Barnett AO, Lomas S, Vullum PE, et al. Flame Spray Pyrolysis of Electrode Materials for Energy Applications. MRS Proceedings. 2015;1747
[98] Bi W, Hu Y, Jiang H, Yu H, Li W, Li C. In-situ synthesized surface N-doped Pt/TiO2 via flame spray pyrolysis with enhanced thermal stability for CO catalytic oxidation. Applied Surface Science. 2019;481:360-8

[99] Babu DJ, Darbandi AJ, Suffner J, Bhattacharya SS, Hahn H. Flame spray synthesis of nano lanthanum strontium manganite for solid oxide fuel cell applications. Transactions of The Indian Institute of Metals. 2011;64:181-4
[100] Simmance K, Thompsett D, Wang W, Thiebaut B. Evaluation of perovskite catalysts prepared by flame spray pyrolysis for three-way catalyst activity under simulated gasoline exhaust feeds. Catalysis Today. 2019;320:40-50
[101] Yu H, Baricci A, Bisello A, Casalegno A, Guetaz L, Bonville L, et al. Strategies to mitigate Pt dissolution in low Pt loading proton exchange membrane fuel cell: I. A gradient Pt particle size design. Electrochimica Acta. 2017;247:1155-68
[102] Yu H, Baricci A, Casalegno A, Guetaz L, Bonville L, Maric R. Strategies to mitigate Pt dissolution in low Pt loading proton exchange membrane fuel cell: II. A gradient Pt loading design. Electrochimica Acta. 2017;247:1169-79
[103] Solakidou M, Georgiou Y, Deligiannakis Y. Double-Nozzle Flame Spray Pyrolysis as a Potent Technology to Engineer Noble Metal-TiO2 Nanophotocatalysts for Efficient H2 Production. Energies. 2021;14:817.
[104] Seo DJ, Ryu KO, Park SB, Kim KY, Song R-H. Synthesis and properties of Ce1−xGdxO2−x/2 solid solution prepared by flame spray pyrolysis. Materials Research Bulletin. 2006;41:359-66
[105] Nagasawa T, Matsumoto K, Minegishi N, Kosaka H. Structural Characterization of Ceria-Supported Pt Nanoparticles by Flame-Assisted Spray Pyrolysis Using a Burner Diffusion Flame. Energy & Fuels. 2021;35:12380-91
[106] Huo J, Hu Y, Jiang H, Huang W, Li C. SnO2 nanorod@TiO2 hybrid material for dye-sensitized solar cells. J Mater Chem A. 2014;2:8266-72
[107] Zhang C, Oliaee SN, Hwang SY, Kong X, Peng Z. A Generic Wet Impregnation Method for Preparing Substrate-Supported Platinum Group Metal and Alloy Nanoparticles with Controlled Particle Morphology. Nano Lett. 2016;16:164-9
[108] Zhang C, Shen X, Pan Y, Peng Z. A review of Pt-based electrocatalysts for oxygen reduction reaction. Frontiers in Energy. 2017;11:268-85
[109] Breitkopf R, Hwang J, Maniei F, Hunt AT. Carbon supported Pt nanomaterials for fuel cell applications using combustion chemical vapor condensation. Nanotechnology. 2003;3:490-2
[110] Daudt NF, Poozhikunnath A, Yu H, Bonville L, Maric R. Nano-sized Pt–NbOx supported on TiN as cost-effective electrocatalyst for oxygen reduction reaction. Materials for Renewable and Sustainable Energy. 2020;9:18.
[111] Roller JM. Flame Synthesis of Nanomaterials for Alternative Energy Applications [Doctoral Dissertation]. https://opencommons.uconn.edu/dissertations/4322014.
[112] Huang S-Y, Ganesan P, Park S, Popov BN. Development of a Titanium Dioxide-Supported Platinum Catalyst with Ultrahigh Stability for Polymer Electrolyte Membrane Fuel Cell Applications. Journal of the American Chemical Society. 2009;131:13898-9
[113] Ding S, Chen H-A, Mekasuwandumrong O, Hülsey MJ, Fu X, He Q, et al. High-temperature flame spray pyrolysis induced stabilization of Pt single-atom catalysts. Applied Catalysis B: Environmental. 2021;281:119471.
[114] Liu J, Ding T, Zhang H, Li G, Cai J, Zhao D, et al. Engineering surface defects and metal–support interactions on Pt/TiO2(B) nanobelts to boost the catalytic oxidation of CO. Catalysis Science & Technology. 2018;8:4934-44
[115] Teleki A, Pratsinis SE. Blue nano titania made in diffusion flames. Phys Chem Chem Phys. 2009;11:3742-7
[116] Wang L, Wan X, Liu S, Xu L, Shui J. Fe-N-C catalysts for PEMFC: Progress towards the commercial application under DOE reference. Journal of Energy Chemistry. 2019;39:77-87

[117] Myles TD, Ouimet R, Kwak D, Maric R. Characterization and performance of proton conducting solid oxide fuel cells manufactured using reactive spray deposition technology. ECS Transactions. 2016;72:17-23
[118] Stollberg DW, Hampikian JM, Riester L, Carter WB. Nanoindentation measurements of combustion CVD Al2O3 and YSZ films. Materials Science and Engineering: A. 2003;359:112-8
[119] Maedler L, Pratsinis SE. Bismuth Oxide Nanoparticles by Flame Spray Pyrolysis. J Am Ceram Soc. 2002;85:1713-8
[120] Zhang S-L, Huang J-Y, Li C-X, Yang G-J, Li C-J. Relationship Between Designed Three-Dimensional YSZ Electrolyte Surface Area and Performance of Solution-Precursor Plasma-Sprayed La0.8Sr0.2MnO3−δ Cathodes. Journal of Thermal Spray Technology. 2016;25:1692-9
[121] Wang L, Wurster P, Gazdzicki P, Roussel M, Sanchez DG, Guétaz L, et al. Investigation of activity and stability of carbon supported oxynitrides with ultra-low Pt concentration as ORR catalyst for PEM fuel cells. Journal of Electroanalytical Chemistry. 2018;819:312-21
[122] Dreyer JAH, Grossmann HK, Chen J, Grieb T, Gong BB, Sit PHL, et al. Preferential oxidation of carbon monoxide over Pt–FeO /CeO2 synthesized by two-nozzle flame spray pyrolysis. Journal of Catalysis. 2015;329:248-61
[123] Lv H, Li D, Strmcnik D, Paulikas AP, Markovic NM, Stamenkovic VR. Recent advances in the design of tailored nanomaterials for efficient oxygen reduction reaction. Nano Energy. 2016;29:149-65
[124] Strobel R, Pratsinis SE. Effect of solvent composition on oxide morphology during flame spray pyrolysis of metal nitrates. Phys Chem Chem Phys. 2011;13:9246-52